The Astronomical Journal, 145:55 (16pp), 2013 March doi:10.1088/0004-6256/145/3/55

CHARACTERIZING THE MID-INFRARED EXTRAGALACTIC SKY WITH *WISE* AND SDSS

Lin Yan[1], E. Donoso[1], Chao-Wei Tsai[1], D. Stern[2], R. J. Assef[2,8], P. Eisenhardt[2], A. W. Blain[3], R. Cutri[1], T. Jarrett[1], S. A. Stanford[4], E. Wright[5], C. Bridge[6], and D. A. Riechers[6,7]
[1] Infrared Processing and Analysis Center, California Institute of Technology, MS 100-22, Pasadena, CA 91125, USA; lyan@ipac.caltech.edu
[2] Jet Propulsion Laboratory, California Institute of Technology, Pasadena, CA 91109, USA
[3] Department of Physics & Astronomy, University of Leicester, University Road, Leicester LE1 7RH, UK
[4] Department of Physics, University of California, Davis, CA 95616, USA
[5] Astronomy Department, University of California, Los Angeles, CA 90095-1547, USA
[6] Astronomy Department, California Institute of Technology, 1200 East California Blvd, Pasadena, CA91125, USA
[7] Astronomy Department, Cornell University, Ithaca, NY 14853, USA
Received 2012 September 7; accepted 2012 December 10; published 2013 January 18

ABSTRACT

The *Wide-field Infrared Survey Explorer* (*WISE*) has completed its all-sky survey in four channels at 3.4–22 μm, detecting hundreds of millions of objects. We merge the *WISE* mid-infrared data with optical data from the Sloan Digital Sky Survey (SDSS) and provide a phenomenological characterization of *WISE* extragalactic sources. *WISE* is most sensitive at 3.4 μm ($W1$) and least sensitive at 22 μm ($W4$). The $W1$ band probes massive early-type galaxies out to $z \gtrsim 1$. This is more distant than SDSS identified early-type galaxies, consistent with the fact that 28% of 3.4 μm sources have faint or no r-band counterparts ($r > 22.2$). In contrast, 92%–95% of 12 μm and 22 μm sources have SDSS optical counterparts with $r \leqslant 22.2$. *WISE* 3.4 μm detects 89.8% of the entire SDSS QSO catalog at $S/N_{W1} > 7\sigma$, but only 18.9% at 22 μm with $S/N_{W4} > 5\sigma$. We show that *WISE* colors alone are effective in isolating stars (or local early-type galaxies), star-forming galaxies, and strong active galactic nuclei (AGNs)/QSOs at $z \lesssim 3$. We highlight three major applications of *WISE* colors: (1) Selection of strong AGNs/QSOs at $z \leqslant 3$ using $W1 - W2 > 0.8$ and $W2 < 15.2$ criteria, producing a better census of this population. The surface density of these strong AGN/QSO candidates is 67.5 ± 0.14 deg^{-2}. (2) Selection of dust-obscured, type-2 AGN/QSO candidates. We show that *WISE* $W1 - W2 > 0.8$, $W2 < 15.2$ combined with $r - W2 > 6$ (Vega) colors can be used to identify type-2 AGN candidates. The fraction of these type-2 AGN candidates is one-third of all *WISE* color-selected AGNs. (3) Selection of ultraluminous infrared galaxies (ULIRGs) at $z \sim 2$ with extremely red colors, $r - W4 > 14$ or well-detected 22 μm sources lacking detections in the 3.4 and 4.6 μm bands. The surface density of $z \sim 2$ ULIRG candidates selected with $r - W4 > 14$ is 0.9 ± 0.07 deg^{-2} at $S/N_{W4} \geqslant 5$ (the corresponding, lowest flux density of 2.5 mJy), which is consistent with that inferred from smaller area *Spitzer* surveys. Optical spectroscopy of a small number of these high-redshift ULIRG candidates confirms our selection, and reveals a possible trend that optically fainter or $r - W4$ redder candidates are at higher redshifts.

Key words: galaxies: evolution – galaxies: high-redshift – galaxies: starburst – infrared: galaxies

Online-only material: color figures

1. INTRODUCTION

With the power of large number statistics, wide-area astronomical surveys in this decade have made many significant discoveries. A new generation of high-precision, wide-area optical imaging surveys is being proposed for the end of this decade to address fundamental questions in cosmology and galaxy formation and to search for extrasolar planets. Most recently, the advent of the *Wide-field Infrared Survey Explorer* (*WISE*; Wright et al. 2010) has provided the community with an unprecedented data set in the mid-infrared. This unique NASA mission mapped the entire sky in four bands at 3.4, 4.6, 12, and 22 μm ($W1$ through $W4$), with 5σ point-source sensitivities better than 0.05, 0.1, 0.75, and 6 mJy, respectively. *WISE* 12 μm images are more than 100 times deeper than previous all-sky infrared survey missions, such as that provided by the *Infrared Astronomical Satellite* (*IRAS*; Neugebauer et al. 1984), while the 3.4 μm data are 1.5 mag (a factor of four in flux density) deeper than the Two-Micron All-Sky Survey (2MASS; Skrutskie et al. 2006) K_s data for sources with spectral energy distributions (SEDs) similar to an A0 star; *WISE* is even more sensitive for red sources like K-stars, early-type galaxies, active galactic nuclei (AGNs), and dust-obscured galaxies.

WISE has made two public data releases, including co-added atlas images and source catalogs. The first was the preliminary release in 2011 April, covering roughly half of the sky, and the second was the all-sky data release in 2012 March, covering the entire sky. Although *WISE* has a significantly smaller aperture and the angular resolution is only half that of *Spitzer*, its unique all-sky coverage enables selection of large samples of extragalactic sources, allowing statistical studies of stellar photospheric emission at 3.4 and 4.6 μm and dust emission at 12 and 22 μm. The primary goal of this paper is to provide an empirical characterization of *WISE* extragalactic sources, and to identify the types of sources which can be isolated using mid-infrared colors. To achieve this goal, we combine *WISE* mid-infrared data with optical data from the Sloan Digital Sky Survey (SDSS) seventh data release (DR7; Abazajian et al. 2009). We characterize the color distributions and source types using broadband photometry and spectroscopic information. The motivation for such a phenomenological study is to give the community a summary of the observational properties and the limitations of two large surveys, particularly for mid-infrared extragalactic objects. More detailed, quantitative analyses of

[8] NASA Postdoctoral Program.

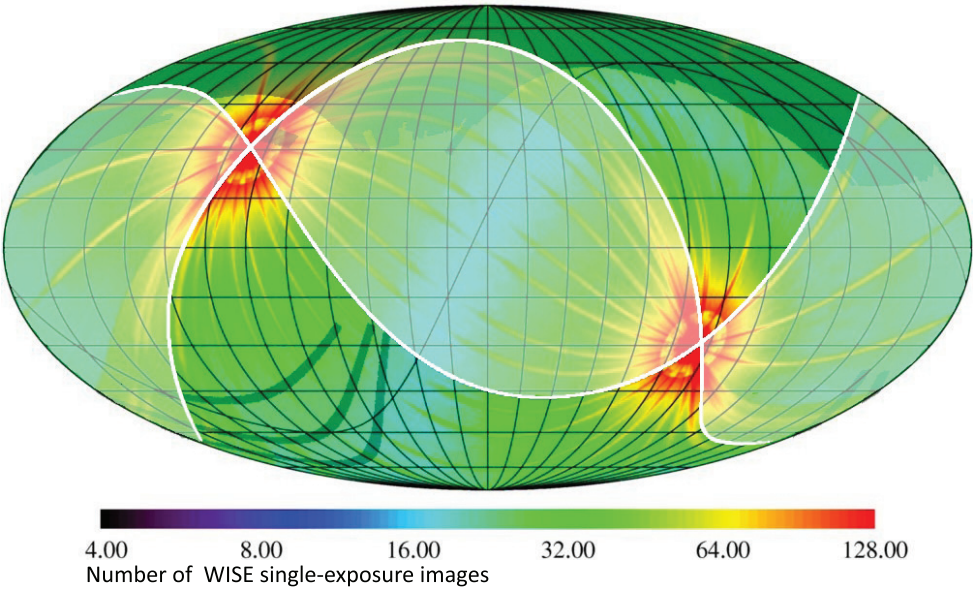

Figure 1. Sky coverage of *WISE* and SDSS DR7 in Galactic Coordinates. The background map shows the *WISE* all-sky depth with colors indicating the number of single-exposure frames at each sky position. The white overlaid area shows the sky region covered by the *WISE* preliminary public data release, covering 57% of the full sky. The dark green region, primarily towards the north Galactic cap, is covered by the SDSS DR7 data. This paper analyzes data drawn from the overlap regions between the *WISE* preliminary public data release and SDSS DR7, a region covering 2344 deg^2.

specific extragalactic populations are discussed in companion papers by the *WISE* extragalactic science team. Specifically, Griffith et al. (2011) and Tsai et al. (2013) discuss *WISE* selection of low-metallicity blue compact dwarf galaxies at $z \lesssim 0.1$. Donoso et al. (2012) examine the origin of 12 μm emission in mid-infrared galaxies at $z \sim 0.1$ using *WISE* data in conjunction with SDSS DR7 spectroscopic data, while Lake et al. (2012) use Keck spectroscopy to study the redshift distribution of flux-limited *WISE* samples. Stern et al. (2012) and Assef et al. (2012) present detailed studies of *WISE*-selected AGN within the Cosmic Evolution Survey (COSMOS) and Boötes fields, respectively, including careful analyses of completeness and reliability of *WISE* AGN selection using $W1 - W2$ color. Eisenhardt et al. (2012) present the first results for $z \sim 2$ ultraluminous infrared galaxies (ULIRGs) discovered by *WISE*. Wu et al. (2012) and L. Yan et al. (in preparation) present the far-infrared properties and SEDs of similarly selected galaxies based on ground-based millimeter and *Herschel* space-based far-infrared data, respectively. Bridge et al. (2012) discuss the interesting Lyα properties of the *WISE* ULIRG population, emphasizing the high rate of extended emission, so-called Lyα blobs. Tsai et al. (2013) and D. Stern et al. (in preparation) present detailed studies of two interesting *WISE*-selected AGN, while Jarrett et al. (2012) and S. Petty et al. (in preparation) study spatially resolved, local ($z < 0.1$) galaxies with *WISE*. Blain et al. (2013) present the *WISE* properties of $z \geqslant 6$ optically selected QSOs. Finally, Gettings et al. (2012) discuss the first results of using *WISE* to identify high-redshift galaxy clusters.

The organization of this paper is as follows. Section 2 describes the *WISE* and SDSS data, including the *WISE* sample selection and the SDSS optical data used by this paper. Section 3 presents the main results, providing the technical details of the catalog matching and summarizing the brightness, color, and photometric redshift distributions for galaxies detected by both *WISE* and SDSS (Section 3.1). We identify the characteristic color criteria which can be used to select large samples of strong AGNs/QSOs (Section 3.2), type-2 AGN candidates (Section 3.3), and potential $z \sim 2$ ULIRGs (Section 3.4). Section 4 summarizes the main conclusions and discusses the implications for future studies using *WISE*. Throughout the paper, we adopt an $\Omega_M = 0.27$, $\Omega_\Lambda = 0.73$, and $H_0 = 71\,\mathrm{km\,s^{-1}\,Mpc^{-1}}$ cosmology.

2. DATA

2.1. WISE−SDSS Sky Coverage

The data used by this paper are drawn from the overlapping sky region where both *WISE* preliminary public release data and SDSS DR7 data are available. Although this area is only one-fourth of the total SDSS area, the number of galaxies included in our analysis is $>10^7$, large enough for the purposes of this paper. Because this paper started with the preliminary release data, we kept the same overlap region between the preliminary release data and SDSS DR7, but the actual *WISE* photometry are taken from the all-sky data release. Figure 1 presents the full-sky coverage map from *WISE*, with colors indicating the number of repeated single exposures at each sky position. Overlaid in the figure are the coverages of the SDSS DR7 data and the *WISE* preliminary release data. The overlap area between DR7 and the *WISE* preliminary release is 2344 deg^2 and defines the area analyzed in the rest of this paper. This area is slightly less than 30% of the total SDSS areal coverage, and is 5.7% of the entire sky.

One characteristic feature of the *WISE* mission is that it does not have uniform depth-of-coverage. For both the preliminary and the all-sky data release, the median depth-of-coverage is 15.65, 15.55, 14.85, and 14.84 exposures at $W1$, $W2$, $W3$, and $W4$, respectively (each single exposure has 11 s). 95% of the sky has coverage $\geqslant$10.82 at $W1$, and $\geqslant$9.90 at $W4$.[9] Taking 10 exposures per position as the depth-of-coverage in $W1$ and $W2$, and nine in $W3$ and $W4$, the 5σ sensitivities are 17.30 mag

[9] See Section 6 in the Explanatory Supplement to the *WISE* All-Sky Data Release Products, http://wise2.ipac.caltech.edu/docs/release/allsky/expsup/index.html.

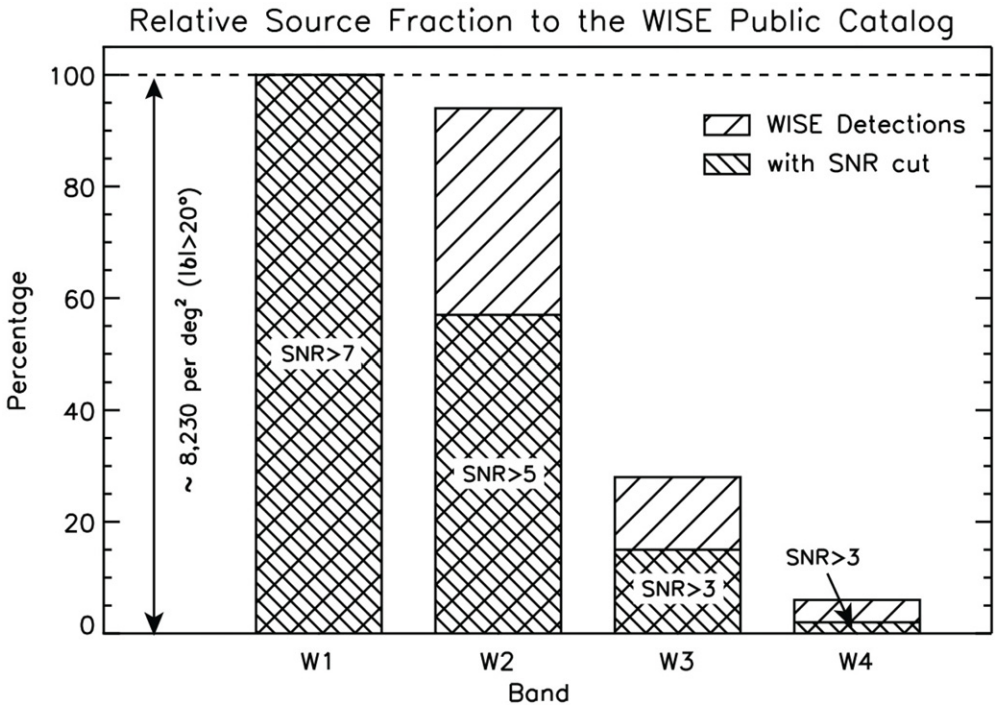

Figure 2. Source densities of our S/N-selected *WISE* samples for the four bands at $|b| > 20^{\circ}$. The leftmost bar, essentially equivalent to the 3.4 μm S/N $\geqslant 7$ catalog, has a source density of 8230 deg^{-2}. The bars illustrate the source fractions with the corresponding S/N cuts at the four bands, relative to the original *WISE* preliminary public release source catalog, which includes all sources with S/N $\geqslant 7$ in at least one band.

(0.037 mJy), 15.84 mag (0.079 mJy), 11.59 mag (0.67 mJy), and 8.00 mag (5.10 mJy) for the four bands, respectively.

2.2. *WISE* Data

We start with the *WISE* preliminary public release source catalog (Cutri et al. 2011).[10] This catalog includes all sources detected in at least one band with photometric signal-to-noise ratio (S/N) $\geqslant 7$ after removing all artifacts. As described in the explanatory supplement to the preliminary data release products, source detection and photometric measurements are performed on all four bands simultaneously. The released catalog contains photometric measurements (or limits) in all four bands.

WISE is the most sensitive at 3.4 μm and the least sensitive at 22 μm; the minimum 5σ sensitivities for these two bands are 0.05 and 6 mJy, respectively. For $f_\nu \propto \nu^\alpha$, the sensitivity ratio $f_\nu(3.4\,\mu\mathrm{m})/f_\nu(22\,\mu\mathrm{m}) = [\nu(3.4\,\mu\mathrm{m})/\nu(22\,\mu\mathrm{m})]^\alpha = 0.0083$ corresponds to a mid-infrared spectral index $\alpha \sim -2.56$. Among all *WISE* $W1$-detected galaxies at the limiting depth of that band, only 2% of the sources are also detected in $W4$, implying extremely red mid-infrared SEDs, redder than $f_\nu \propto \lambda^{2.56}$.

The public released catalog contains a very small number of sources which are detected only in $W3$ and/or $W4$, but not in $W1$ and/or $W2$ (e.g., Eisenhardt et al. 2012). Due to the large sensitivity differences between $W1$ and $W4$, the entire catalog is essentially a 3.4 μm-selected sample with S/N $\geqslant 7$ ($\sigma_{W1} \sim 0.15$); only 0.16% of the catalog is very faint in $W1$ but bright in one of the other three *WISE* bands (e.g., S/N$_{W1} < 7$, but S/N > 7 for any of the other three bands). Therefore, we call this original catalog from the *WISE* data archive, without any additional cuts, the $W1$ sample. Many sources in this preliminary public release catalog have S/N$_{W1} > 7$, but low S/N in the other three *WISE* bands. When we study the color distributions, it becomes necessary to require the color errors to be small relative to the range of colors. Specifically, the $W1 - W2$ color for *WISE* galaxies roughly spans the narrow range, 0 to 2. We require the errors in $W1 - W2$ to be less than 0.27 mag, meaning that we need a source catalog with S/N$_{W2} \geqslant 5$ (corresponding to $\sigma_{W2} < 0.22$ mag). A similar argument is applied to the $W2 - W3$ colors, which have a larger spread of 0.5–5. In this case, we require S/N$_{W3} \geqslant 3$ ($\sigma_{W3} < 0.35$ mag). In summary, to obtain meaningful color distributions, we base our analyses below on the following three source samples: the original $W1$ sample (S/N$_{W1} \geqslant 7$), a $W1/2$ sample (S/N$_{W1} \geqslant 7$ and S/N$_{W2} \geqslant 5$), and a $W1/2/3$ sample (S/N$_{W1} \geqslant 7$, S/N$_{W2} \geqslant 5$, and S/N$_{W3} \geqslant 3$).

Figure 2 shows the source fraction in each of the above three samples relative to the four-band merged, public released catalog. When applying additional photometric S/N cuts, the source sample sizes become increasingly smaller. At S/N $\geqslant 5$, 4.6 μm sources are only 57% of the $W1$ sample. At S/N $\geqslant 3$, this fraction is only 15% and 2% at 12 μm and 22 μm, respectively. In the sense of source surface density, the $W1$ sample has ~8230 sources per deg^2, whereas the $W1/2$ and $W1/2/3$ samples have only 4700 and 1235 sources per deg^2, respectively. For comparison, the source surface density in the SDSS photometric catalog is about 27,300 sources per deg^2, over three times higher than that of *WISE* 3.4 μm. This is because SDSS detects many more low-luminosity (low-mass) galaxies than *WISE* (see, e.g., Donoso et al. 2012).

For the three samples specifically selected for this paper, S/N$_{W1} = 7$ corresponds to apparent magnitudes between 16.8 and 17.6 mag (0.058–0.028 mJy), S/N$_{W2} = 5$ to 15.9–16.5 mag (0.075–0.043 mJy), and S/N$_{W3} = 3$ to the limiting magnitudes of 12.2–12.8 mag (0.38–0.22 mJy).

[10] A detailed description of the catalog can be found in the Explanatory Supplement to the *WISE* Preliminary Data Release Products at http://wise2.ipac.caltech.edu/docs/release/prelim/expsup/.

WISE photometry is calibrated relative to measurements of standard stars, using the Vega magnitude system. The conversion factors to the AB system ($m_{\rm AB} \equiv m_{\rm Vega} + \Delta m$) are 2.683 ($W1$), 3.319 ($W2$), 5.242 ($W3$), and 6.604 ($W4$); equivalently, zero magnitude corresponds to 309.5, 171.79, 31.676, and 8.36 Jy for the four bands, respectively (Wright et al. 2010; Jarrett et al. 2011). SDSS photometry directly output from the SDSS archive is in the asinh magnitude system. We translate asinh magnitudes into the AB system using information provided by SDSS.[11] When calculating SDSS−*WISE* colors, we convert SDSS photometry to the Vega system using $r({\rm AB}) - r({\rm Vega}) = 0.16$ (Fukugita, Shimasaku & Ichikawa 1995). Throughout this paper, *WISE* magnitudes are in the Vega system and SDSS magnitudes are in the AB system, but all colors are in the Vega system.

2.3. SDSS Data

This paper uses the SDSS DR7 data (Abazajian et al. 2009), including the photometric catalog, the main galaxy spectroscopic catalog[12] (Brinchmann et al. 2004), the luminous red galaxy (LRG) spectroscopic sample (Eisenstein et al. 2001), and the QSO sample (Schneider et al. 2010). The DR7 legacy survey catalog covers 8423 deg^2 and contains 230 million sources. The main galaxy spectroscopic catalog is generated jointly by the Max-Planck-Institut fur Astrophysik and the Johns Hopkins University (MPA-JHU DR7 main galaxy catalog; Brinchmann et al. 2004). It consists of almost 10^6 galaxies with Petrosian (1976) magnitudes brighter than $r = 17.77$ for which various derived physical parameters are readily available. We adopt the following classification criteria as in Kauffmann et al. (2003): star-forming (SF) galaxies are defined as having $\log[{\rm O\,III}/{\rm H}\beta] < 1.3 + 0.61\log[{\rm N\,II}/{\rm H}\alpha - 0.05]$ (Equation (1) in Kauffmann et al. 2003); AGNs (Seyfert and LINERs) are defined as having $\log([{\rm O\,III}]/{\rm H}\beta) > 1.19 + 0.61/[\log([{\rm N\,II}]/{\rm H}\alpha) - 0.47]$ (Equation (5) in Kewley et al. 2001); and composite systems are defined as having $\log([{\rm O\,III}]/{\rm H}\beta)$ between the two values described by the above equations. These SF galaxy and AGN definitions are used in Section 3.2 when we utilize SDSS spectra to classify *WISE* sources. When based on *WISE* data alone, we do not use these definitions. Two LRG samples are selected in color–magnitude space: one to $r = 19.2$ (roughly volume-limited, to $z = 0.38$) and one to $r = 19.5$ (flux-limited, to $z = 0.55$) (Eisenstein et al. 2001). The QSO sample is selected by their non-stellar colors or FIRST (Faint Images of the Radio Sky at Twenty-cm; Becker et al. 1995) radio emission to $i = 19.1$ for $z < 3$ and to $i = 20.2$ for $3 < z < 5.5$ (Richards et al. 2002).

In addition, all SDSS photometric redshifts (when spectroscopic redshifts are not available) used in the sections below are the ones derived based on the neural network method (Oyaizu et al. 2008). We caution that, in general, broadband photometric redshifts are highly uncertain for strong type-1 AGNs/QSOs (Assef et al. 2010; Brodwin et al. 2006). These strong type-1 AGNs from SDSS have the most complete spectroscopic redshifts.

3. ANALYSIS AND RESULTS

3.1. Apparent Magnitude and Redshift Distributions

The *WISE* 3.4 and 4.6 μm bands primarily sample emission from stellar photospheres, whereas the 12 and 22 μm bands are more sensitive to dust emission heated by stars and accreting black holes. Therefore, *WISE* readily identifies a variety of galaxy populations in the mid-infrared sky. To characterize these populations, we first address several basic properties of the matched *WISE*−SDSS catalog, including optical brightness distributions, redshifts, the fraction of *WISE* sources undetected or with very faint optical counterparts, and optical through mid-infrared colors of matched sources.

We carried out source matching between *WISE* and SDSS DR7 with a matching radius of 3″. This is based on the fact that the *WISE* angular resolutions are 6.″1, 6.″4, 6.″5, and 12″ for the four bands, respectively. Figure 3 shows the percentage of *WISE* sources with SDSS r-band optical counterparts for the four *WISE* bands. To a depth of $r = 22.6$, corresponding to the 50% completeness depth of SDSS (Abazajian et al. 2009), 91% of the $W1/2/3$ and 96% of the $W1/2/3/4$ (S/N$_{W4} \geqslant 3$) samples have optical counterparts. In contrast, only 72% and 86% of the $W1$ and the $W1/2$ samples have optical counterparts with $r < 22.6$. This implies that the bulk of 12 and 22 μm galaxies are dusty SF galaxies and AGNs at low redshifts ($z \sim 0.1$–0.3), whereas 15%–25% of 3.4 and 4.6 μm sources could be massive early-type galaxies which are fainter than the SDSS photometric limits and are at $z \geqslant 1$. Indeed, Gettings et al. (2012) report on a *WISE*-selected galaxy cluster at $z = 0.99$ which is well detected in $W1$ and $W2$ but is undetected by SDSS.

Figure 4 shows the optical brightness and photometric redshift distributions for the mid-infrared sources detected in the four bands. It is clear that *WISE* 22 μm sources have corresponding optical magnitudes which peak at $r \sim 19$, 1 mag brighter than the peaks for the $W1$, $W2$, and $W3$ samples. For comparison, the parent SDSS photometric catalog continues to rise until completeness causes an apparent drop at $r \sim 22$. This confirms that SDSS detects many more low-mass, low-luminosity galaxies than *WISE* and the bulk of *WISE* galaxies with optical counterparts are relatively local, at $0.1 < z < 0.3$.

About 28% and 14% of *WISE* 3.4 μm and 4.6 μm sources are very faint or without any optical counterparts in the SDSS photometric catalog. These optically faint 3.4 μm galaxies are predominantly massive early-type galaxies at $z \gtrsim 1$, though heavily obscured galaxies and AGNs also contribute at some level. Figure 5 examines the $W1 - W2$ colors of this optically faint population, showing that $W1$ sources with very faint r-band magnitudes ($r > 22.6$) have redder $W1 - W2$ colors than optically brighter $W1$ sources. As discussed below and shown with color–redshift tracks for galaxy templates from Assef et al. (2010), redder $W1 - W2$ color is an indicator of early-type and SF galaxies being at higher redshifts, $z \gtrsim 1$.

What types of galaxies are detected by *WISE* at 3.4 and 22 microns? One way to answer this is to calculate expected *WISE* magnitudes as a function of redshift using empirical galaxy templates. Figure 6 shows the expected $W1$ and $W2$ magnitudes for an early-type galaxy template, as well as $W3$ and $W4$ magnitudes for an infrared bright galaxy (IRAS 19254−7245) as a function of redshift. This figure suggests that ignoring evolution, L^* early-type galaxies should be visible in *WISE* 3.4 μm data out to redshifts of 1.5–2. Another important result emphasized by Figure 6 is that the observed $W1$ magnitudes do not change significantly over $z \sim 0.5$–1.5 for early-type galaxies; this benevolent k-correction has been noted repeatedly for the similar 3.6 μm band of *Spitzer* (e.g., Eisenhardt et al. 2008; Mancone et al. 2010; Galametz et al. 2012). In contrast, optical r-band magnitudes steeply decline in brightness with redshift.

[11] See http://www.sdss.org/DR7/algorithms/fluxcal.html.
[12] See http://www.mpa-garching.mpg.de/SDSS/DR7/.

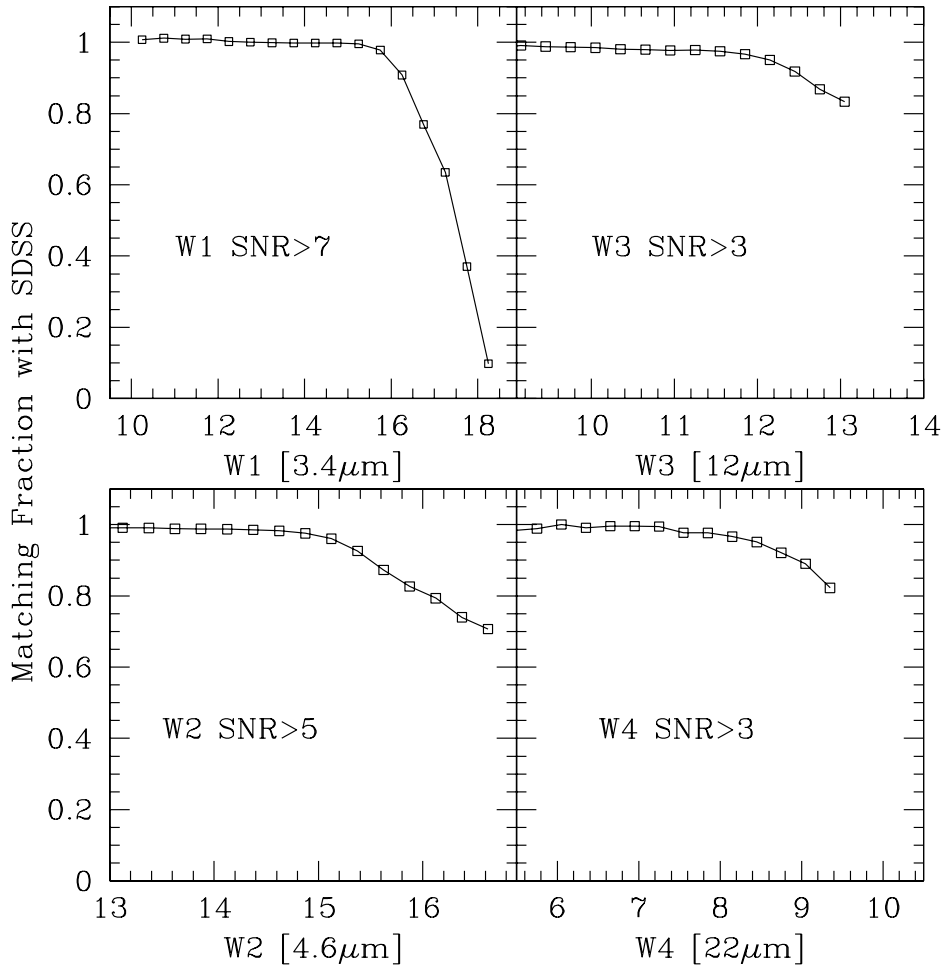

Figure 3. Percentage of *WISE* sources matched with SDSS photometric catalog as a function of *WISE* magnitude.

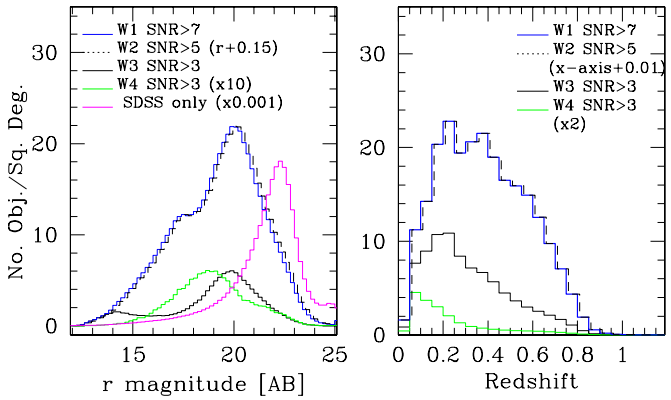

Figure 4. *r*-band magnitude and photometric redshift distributions for the *WISE*−SDSS matched sources from the four *WISE* samples. For both panels, the distributions for *W*1 and *W*1/2 samples are *indistinguishable*, with the *W*1 sample in blue and the *W*1/2 sample in green. For the visual clarity, we slightly shifted the *W*1/2 sample along the *x*-axis as labeled in the figure legend. In the left panel, for the *W*1/2/3/4 sample, we scaled the *y*-axis by a factor of 10 for visual clarity. Similarly, in the right panel, the *y*-axis for the *W*1/2/3/4 sample is scaled by 2. For comparison, we also plot the *r*-band magnitude distribution for the full SDSS photometric catalog (scaled down by a factor of 1000). Note that SDSS optical magnitudes are in the AB system, calculated from SDSS asinh magnitudes. The *r*-band magnitude histograms have a bin size of 0.2 mag. The majority of 12 μm sources have bright SDSS optical counterparts and are at low redshifts ($z \sim 0.2$).

(A color version of this figure is available in the online journal.)

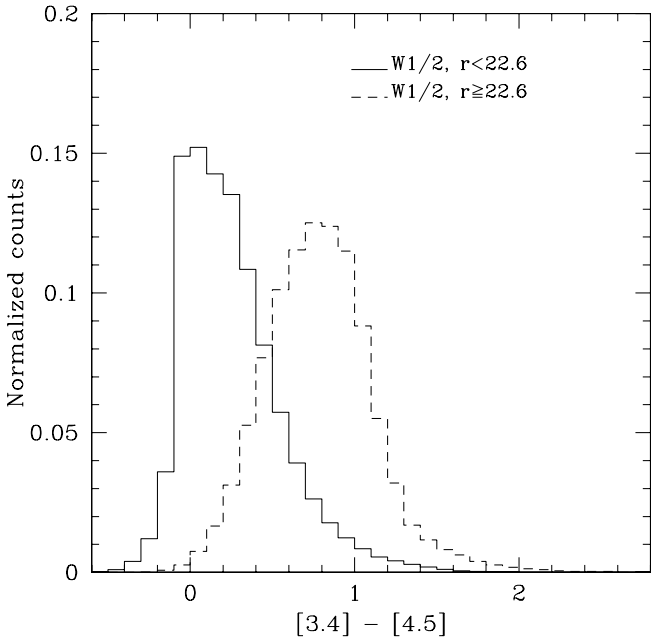

Figure 5. Normalized $W1 - W2$ color distribution for $W1/2$ sample with bright optical counterparts (solid line; $r < 22.6$) compared to sources with faint or undetected optical counterparts in the SDSS data ($r \geqslant 22.6$).

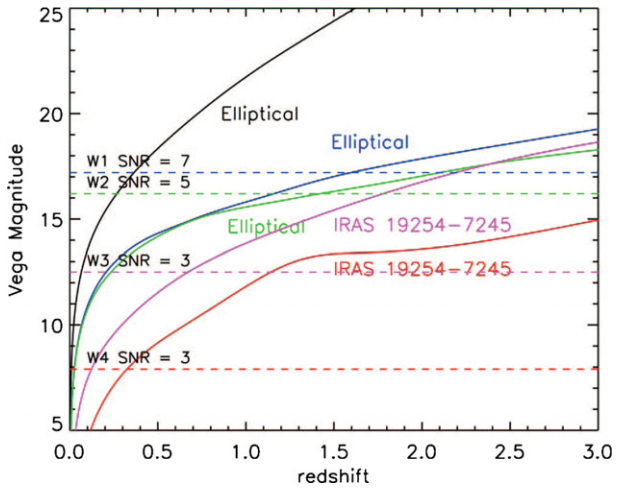

Figure 6. Predicted *r*-, $W1$-, $W2$-, $W3$-, and $W4$-band magnitude as a function of redshift (corresponding to black, blue, green, magenta, and red lines, respectively) using two empirical galaxy SED templates, elliptical galaxy and IRAS 19254−7245. For the early-type galaxy, the template is normalized to an L^* galaxy at $z = 0.043$ with $L_K = 3.5 \times 10^{11}\ L_\odot$ (Lin et al. 2004; Mancone et al. 2010). Minimum *WISE* sensitivity limits are shown as dashed horizontal lines. This shows that *WISE* 3.4 μm images are sensitive to typical early-type galaxies out to $z \sim 1$; this sensitivity is enhanced for more luminous early-type galaxies and/or higher ecliptic latitude fields where the *WISE* coverage is deeper.

Figure 7 illustrates how $W1$ and $W4$ magnitudes change with optical brightness, *r*, and photometric redshift. $W1$ traces *r* until $r \sim 20$–21, at which point $W1$ magnitudes remain within a narrow range of 15.8–16.8 mag, while optical brightness becomes increasingly fainter, stretching over three magnitudes. Figures 6 and 7 illustrate the same effect, i.e., most galaxy SEDs have very steep slopes at ultraviolet through optical wavelengths, and much shallower slopes in the near-infrared. The turnover at $r \sim 20$ in Figure 7 implies that the bulk of $W1$ sources are low-redshift ($z < 0.5$), typical SDSS-detected galaxies, and $W1$ sources with $r \gtrsim 20$ tend to be at higher redshifts ($z \sim 0.5$–2).

3.2. Separating Powerful AGNs/QSOs at $z \leqslant 3$ from Galaxies

With four-band mid-infrared photometry, can *WISE* colors alone provide diagnostics for different types of sources as well as crude redshift information? Figure 8 addresses this question by showing $W1 - W2$ versus $W2 - W3$ colors for the $W1/2/3$ sample. The three high source density regions are as follows: (1) the stellar locus with both colors near zero; at mid-infrared wavelengths, emission from Galactic stars from spectral class O through ∼T3 is dominated by the Rayleigh–Jeans tail of the blackbody spectrum, thereby yielding Vega-system colors near zero for most Galactic stars (note that pure elliptical galaxies with no dust at $z \leqslant 0.1$ also sit near the stellar locus); (2) the red $W1 - W2$ cloud with $W1 - W2 > 0.8$; and (3) the bluer $W1 - W2$ sequence, spanning a wide range in $W2 - W3$ color. Here we do not see any extremely cool brown dwarfs with very red $W1 - W2$ color due to methane absorption since such sources are very faint in $W3$, and thus are excluded in our $W1/2/3$ sample (Kirkpatrick et al. 2011).

What is the physical basis of the color–color distribution shown in Figure 8? Figures 9 through 11 examine this question from different angles. Figure 9 shows empirical galaxy and AGN templates from 0.03 to 30 μm based on ∼20,000 objects with multi-wavelength data in the NOAO Deep Wide-Field Survey (Assef et al. 2010). For systems with strong nuclear heating, the mid-infrared SEDs tend to be roughly a rising power law, resulting in $W1 - W2 > 0.8$. For systems with dominant stellar emission at $z < 1$, this color is smaller because the 3.4 μm band is sampling below the 1.6 μm H^- opacity peak of the stellar emission, making the $W1 - W2$ color bluer; at $z > 1$, the 3.4 μm band samples below the near-infrared stellar peak, getting fainter, thereby providing redder $W1 - W2$ colors.

Figure 10 shows the $W1 - W2$ and $W2 - W3$ color tracks as a function of redshift calculated using the set of SED templates of Assef et al. (2010), the Arp 220 SED template of Polletta et al. (2007), and the IRAS 15250+3609 template of Vega et al. (2008). The model colors clearly do not span the full range of observed values in Figure 8. The assumed SED templates, generated from optical and *Spitzer* observations, are by no means complete. These templates include elliptical galaxies, star-forming Sbc- and Im-type galaxies, type-1 AGNs, and local ULIRGs Arp 220 and IRAS 15250+3609. The AGN tracks have three different dust obscuration factors; dust-obscured ones are type-2 AGNs.

As opposed to Figure 10 which shows *WISE* colors based on SED templates, Figure 11 is the color–color plot for known

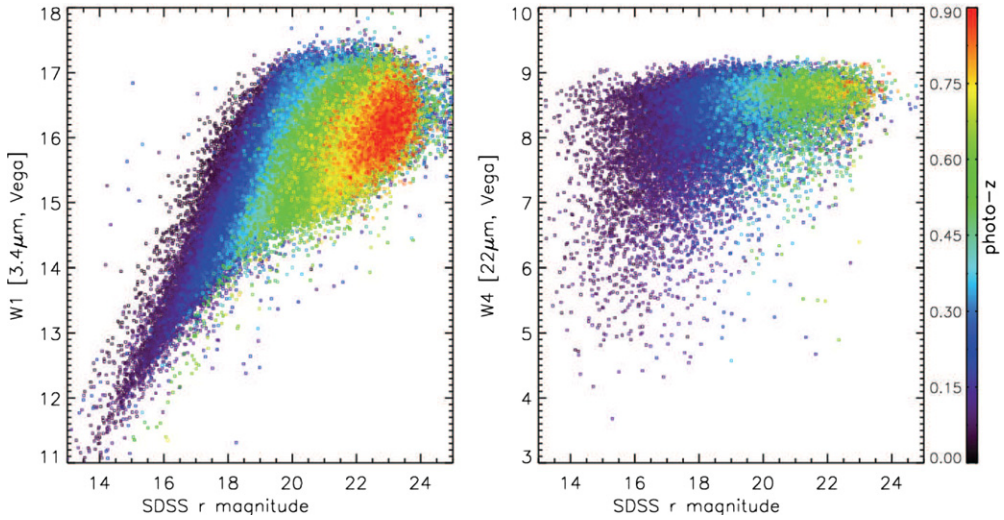

Figure 7. *WISE* 3.4 μm and 22 μm magnitude as a function of optical *r*-band magnitude. The colors indicate photometric redshifts taken from the SDSS catalog. As expected, optically fainter galaxies, i.e., sources with redder $r - W1$ or $r - W4$ colors tend to be at higher redshifts.

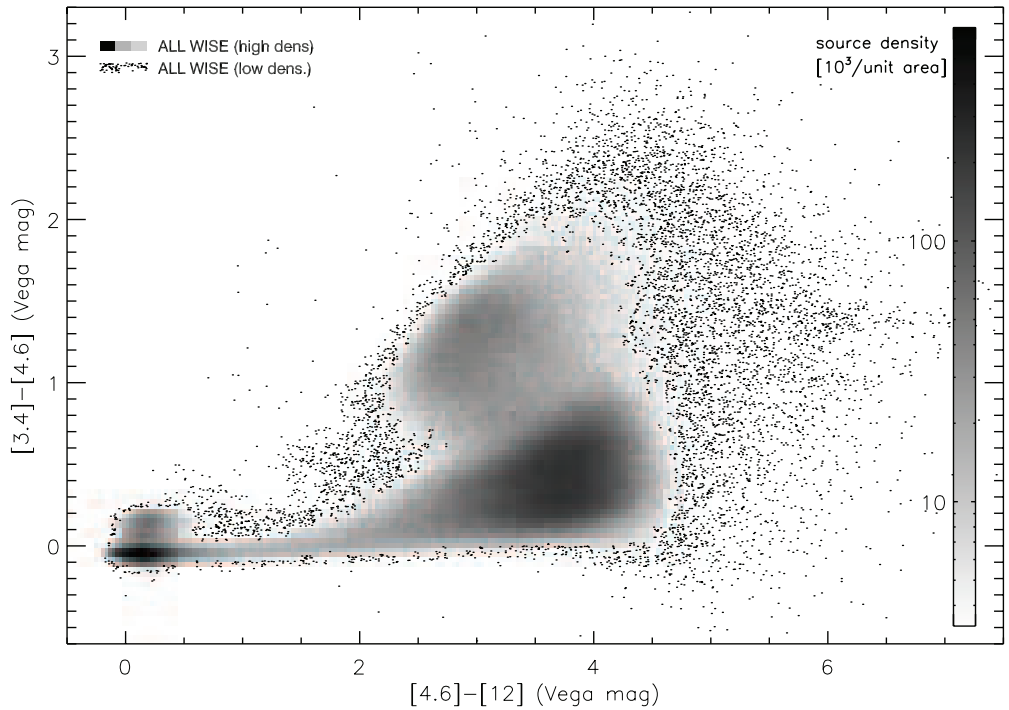

Figure 8. Color–color distribution of *WISE* sources from the 12 μm-selected $W1/2/3$ sample. To illustrate the large range in source density in color–color space, we combine a gray-scale plot for high concentration regions (see scale bar on right) and individual points for low source density regions.

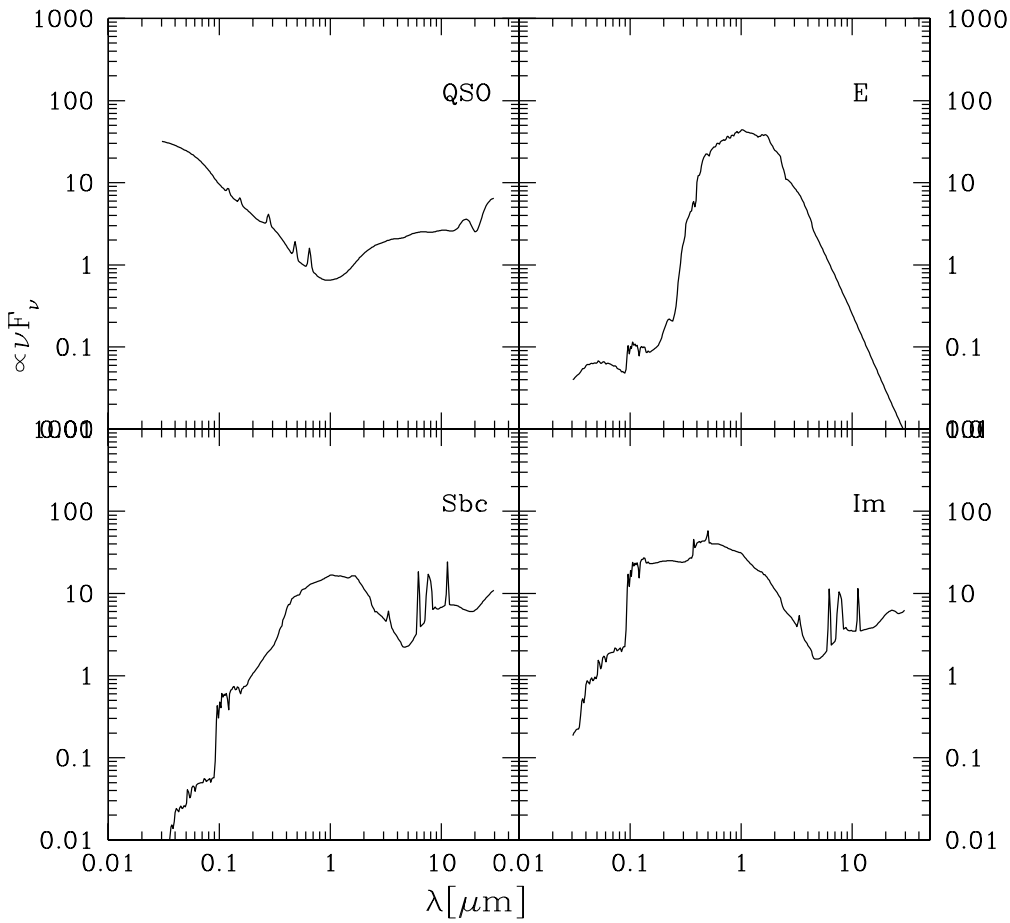

Figure 9. Empirical templates for quasars and normal galaxies from Assef et al. (2010). The major difference between galaxies and AGN is at 1–2 μm: AGNs have a minimum in that wavelength range, while galaxies have a peak in that wavelength range. Star-forming and passive galaxies are easily distinguished from their longer-wavelength data ($\gtrsim 4\,\mu$m).

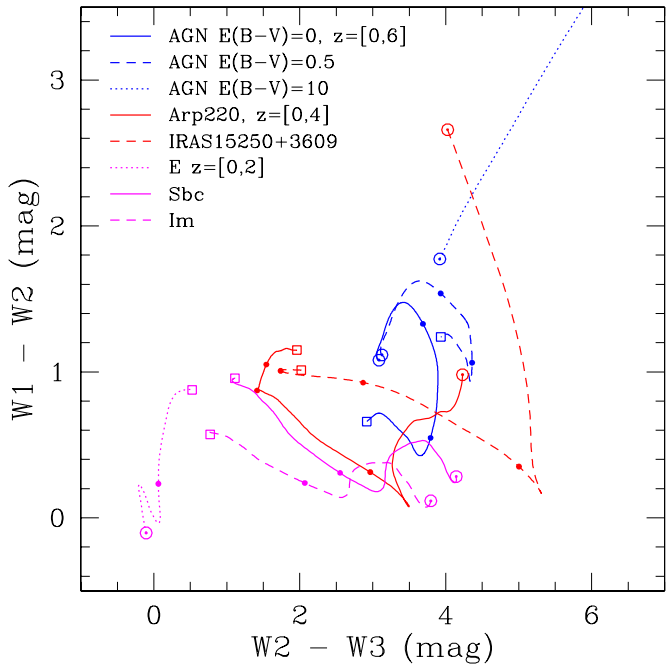

Figure 10. Color–color tracks as a function of redshift for several galaxy and AGN templates taken from Polletta et al. (2007), Vega et al. (2008), and Assef et al. (2010). The blue tracks are for AGNs with target symbols indicating $z = 0$, black dots for $z = 2$, 4, and open squares for $z = 6$. The AGN tracks are shown with three different dust obscuration factors. The red tracks are for the local ULIRGs Arp 220 and IRAS 15250+3609 with target symbols for $z = 0$, solid dots for $z = 1$, 2, 3, and open squares for $z = 4$. The magenta tracks are for normal galaxy templates with target symbols for $z = 0$, solid dots for $z = 1$, and open squares for $z = 2$.

(A color version of this figure is available in the online journal.)

sources. Specifically, we plot SDSS spectroscopically classified sources, including SF galaxies, galaxies hosting AGN, SF/AGN composite systems, LRGs, QSOs, and $z \gtrsim 2$ *WISE*-selected ULIRGs. These figures enable us to conclude that *WISE* colors alone are effective in separating strong AGNs from SF galaxies, and in separating stars from extragalactic sources (other than early-type galaxies at very low-redshift).

Figures 8 through 11 all suggest one unique application of *WISE* data over the entire sky—selecting strong AGN/QSO candidates at $z < 3$ using $W1 - W2$ color. Using mid-IR colors to select AGNs has been noted earlier in *Spitzer* studies over relatively small areas and with much smaller AGN samples (e.g., Lacy et al. 2004; Stern et al. 2005). The selection of $W1 - W2$ method, briefly discussed in Jarrett et al. (2011), is tested and discussed in detail in Stern et al. (2012) and Assef et al. (2012) (see also Ashby et al. 2009; Assef et al. 2010; Eckart et al. 2010; Edelson & Malkan 2012; Massaro et al. 2012; Wu et al. 2012; Mateos et al. 2012). With the current analysis, we, for the first time, investigate this simple selection criterion using the wide-area, large spectroscopic database of SDSS. $W1 - W2$ versus $W2 - W3$ is plotted in Figure 12 for SDSS spectroscopically confirmed QSOs, color coded by redshift. Normal, SF galaxies are also plotted. We see that QSOs at $z \leqslant 3$ mostly have $W1 - W2 \geqslant 0.8$, and are reasonably well separated from SF galaxies. However, $z \sim 3$–5 QSOs have bluer $W1 - W2$ colors due to the 3.4 and 4.6 μm filters sampling rest-frame optical wavelengths, making such quasars difficult to distinguish from normal galaxies based on mid-IR colors alone. A similar issue with *Spitzer* selection of distant quasars was pointed out by Assef et al. (2010). The selected AGN candidate sample has two unique features: (1) it provides a more complete selection of QSOs, particularly at $z \sim 2$–3, where the

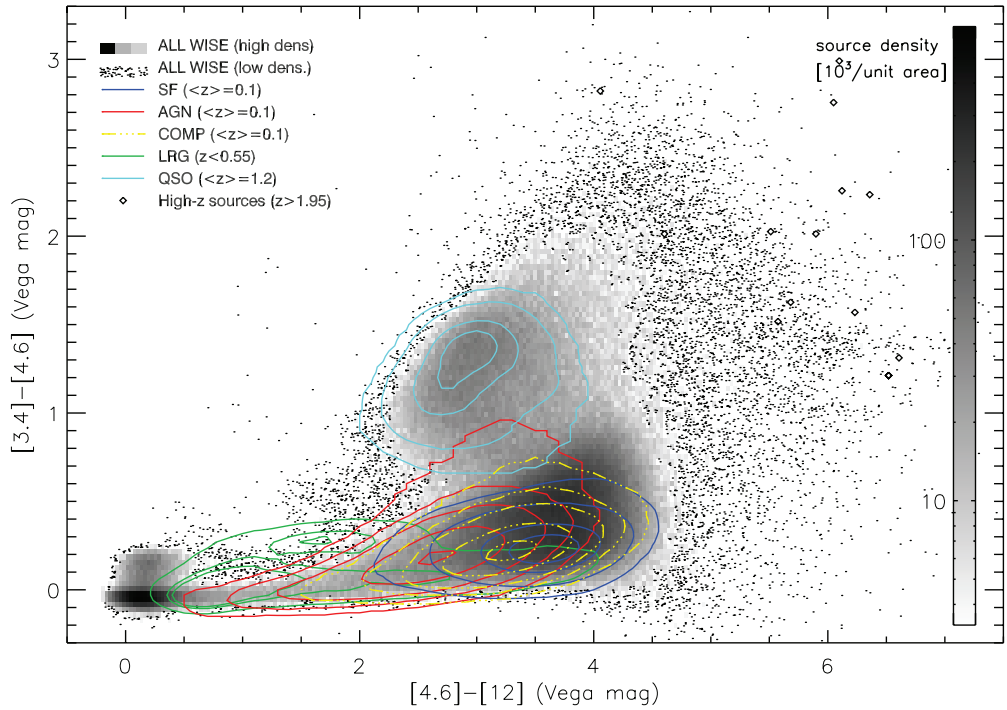

Figure 11. Same as Figure 8, with source classifications indicated, based on the SDSS DR7 spectroscopic galaxy catalog (see text for details). Spectroscopic confirmed QSOs and LRGs are also plotted. The color contours indicate sources which have been classified as star-forming galaxies (SF, blue), Seyfert AGNs (red), composite systems (yellow), LRGs (green), and bright QSOs (cyan). These color contours are used to visually illustrate the concentrations of source distributions in this color–color space. Additionally, we plot several extremely red *WISE*-selected ULIRGs at $z \gtrsim 2$ from Eisenhardt et al. (2012), D. Stern et al. (in preparation), Bridge et al. (2012), Wu et al. (2012), and L. Yan et al. (in preparation).

(A color version of this figure is available in the online journal.)

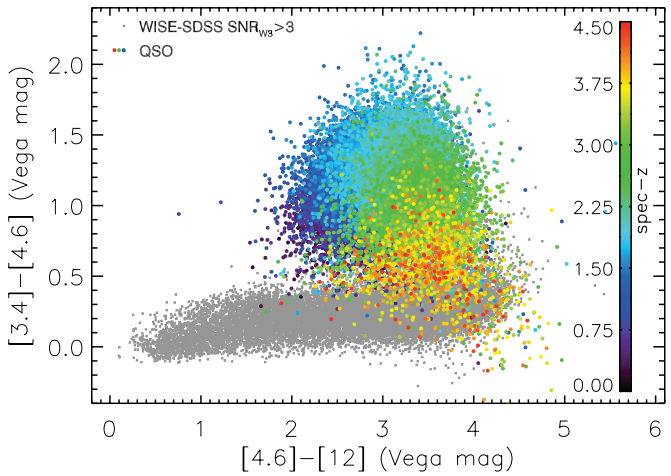

Figure 12. *WISE* color–color distribution for SDSS spectroscopically confirmed quasars, color coded by redshift. Gray points are normal star-forming galaxies. A simple $W1-W2$ color cut efficiently and robustly separates quasars at $z \lesssim 3$ from normal galaxies. Higher redshift quasars, however, enter into the galaxy locus in this color–color diagram.

SDSS optical color method has issues (Richards et al. 2002; Schneider et al. 2010); and (2) it is less affected by dust than optical selection methods, and thus is more sensitive to obscured, type-2 AGNs.

In addition to the color criterion of $W1-W2>0.8$, another important condition for selecting AGN with high completeness and reliability is $W2$ magnitude and S/N limits (see Stern et al. 2012; Assef et al. 2012 for the full details). Using the deep, multi-wavelength data in COSMOS (Scoville et al. 2007), Stern et al. (2012) found that $W1-W2>0.8$ in combination with $W2<15.05$ at S/N >10 identifies 78% of *Spitzer* mid-IR AGN candidates (as the truth sample) with a reliability of 95%. Assef et al. (2012) use higher latitude *WISE* data in the wider-area Boötes field to further investigate the completeness and reliability of the *WISE* AGN selection as functions of magnitude and S/N. As shown in Figure 10 and discussed in Section 3.1, optically faint, high-redshift elliptical and Sbc galaxies tend to have very red $W1-W2$ colors. These sources are contaminants to *WISE* AGNs based on a pure $W1-W2>0.8$ color cut. To limit the contamination, D. Stern et al. (in preparation) and Assef et al. (2012) found that $W2<15.2$ at the number of sky coverage $\geqslant$15 can achieve completeness of 74% and reliability of 89%. Here similar to Stern et al. (2012), the reliability and completeness of *WISE* AGN sample are derived based on using the *Spitzer* color-selected mid-IR AGNs as the truth sample. For our chosen *WISE* + SDSS overlap sub-region, more than 80% of the sky have the coverage $\geqslant$15, and 99% have the coverage $\geqslant$10. At $W2=15.2$, the median source S/N and the number sky coverage are 12 and 22, respectively. Therefore, for our analysis of *WISE* AGNs throughout this paper, we adopt $W2<15.2$ criterion. Our AGN selection criteria of $W1-W2>0.8$, $W2<15.2$ should maintain a reasonable completeness and a good reliability.

What is the source density of *WISE*-selected sources? In the large, high Galactic latitude *WISE*−SDSS overlap area we analyze here, the $W1/2/3$ sample contains 12% Galactic stars, 12% luminous AGN candidates, and 70% normal galaxies (possibly containing weak AGNs). The remaining 6% of $W3$ sources are extremely red, with either $W2-W3\geqslant 4.5$ or $W1-W2\geqslant 1.8$. These present a rare population of red objects, and are likely dusty systems at high redshift (see Section 3.4). With the selection of $W1-W2>0.8$, $W2<15.2$, the *WISE* AGN/QSO candidates have a surface density of 67.5 ± 0.14 deg^{-2}. Considering only the optically bright subsample, with $r<21$, the AGN candidate surface density is 35 deg^{-2}. For comparison, Stern et al. (2012) find 61.9 ± 5.4 deg^{-2} AGN candidates with 95% reliability for $W2<15.05$, and Assef et al. (2012) find 137 ± 4 deg^{-2} candidates for $W2<17.11$.

SDSS spectroscopic QSOs are optically bright sources. What is the fraction of this population detected by *WISE* 3.4 and 22 μm? Figure 13 addresses this question. Overall, *WISE* detects a high fraction of SDSS QSOs from DR7 Schneider et al. (2010) catalog, and $z>5.7$ QSOs from Fan et al. (2006), Jiang et al. (2009), Willott et al. (2009), and Willott et al. (2010). Of the entire QSO sample, only 18.9% have $W4$ detections at S/N $>5\sigma$, and, much higher fraction, 89.8% have $W1$ detections at S/N $>7\sigma$. We note that *WISE* $W1$ is quite sensitive in detecting $z\geqslant5.8$ QSOs, with a detection rate of $\sim$50%, as shown in the bottom panel of Figure 13. In particular, the highest redshift quasar currently known, ULAS J1120+0461 at $z=7.085$ (Mortlock et al. 2011), is also detected by *WISE* 3.4 μm. Blain et al. (2013) present a detailed discussion of the *WISE* properties of $z\geqslant6$ optically selected QSOs.

3.3. Type-2 AGN Candidates

WISE is very sensitive to dust-obscured objects. This naturally leads to two questions: (1) Can *WISE* colors be used to identify type-2 AGNs and (2) What is the relative fraction of type-1 and type-2 QSO/AGNs selected by *WISE*? One simple way to understand the *WISE* colors of extragalactic sources is to compare mid-IR colors of SDSS unresolved, point sources (including QSOs, stars, and compact galaxies) with that of extended galaxies (including type-2 AGNs and normal galaxies). Figure 14 illustrates this comparison, showing clear separation between strong QSOs and SF galaxies. Here we take the SDSS photometric catalog, and separate sources by their morphological types—unresolved point sources versus extended galaxies. This list is then matched with the *WISE* catalog. We do not apply any *WISE* magnitude cut since our purpose is to show the difference in mid-IR color distributions of SDSS extended versus pointed sources. To ensure reliable star/galaxy classification, we require $r<21$ (e.g., 95% reliability quoted in Table 2 in Stoughton et al. 2002). *WISE* colors of unresolved sources (e.g., Galactic stars and quasars) are clearly separated from extended galaxies. Furthermore, in terms of unresolved SDSS sources, note that the Galactic stars (at the origin) are clearly distinct from the unresolved quasars (with redder mid-infrared colors).

One cautionary note about type-2 AGN is that any discussion and conclusions will depend how such sources are defined. In the current analysis, we define two type-2 AGN samples. The first sample is the AGN candidates with $W1-W2>0.8$, $W2<15.2$, and with extended SDSS r-band morphologies (SDSS TYPE $=3$; $r<21$). In general, AGNs have two components: extended galaxy and central accreting black holes. For strong AGNs, the central black hole emission dominates over the extended component in type-1 AGNs, but not in type-2. Here we adopt the morphology criterion for our selection. Unfortunately, this definition only works for optically bright AGN candidates with spatially resolved host galaxies in the SDSS data. It is also worth noting that mid-IR color criteria for AGNs tend to

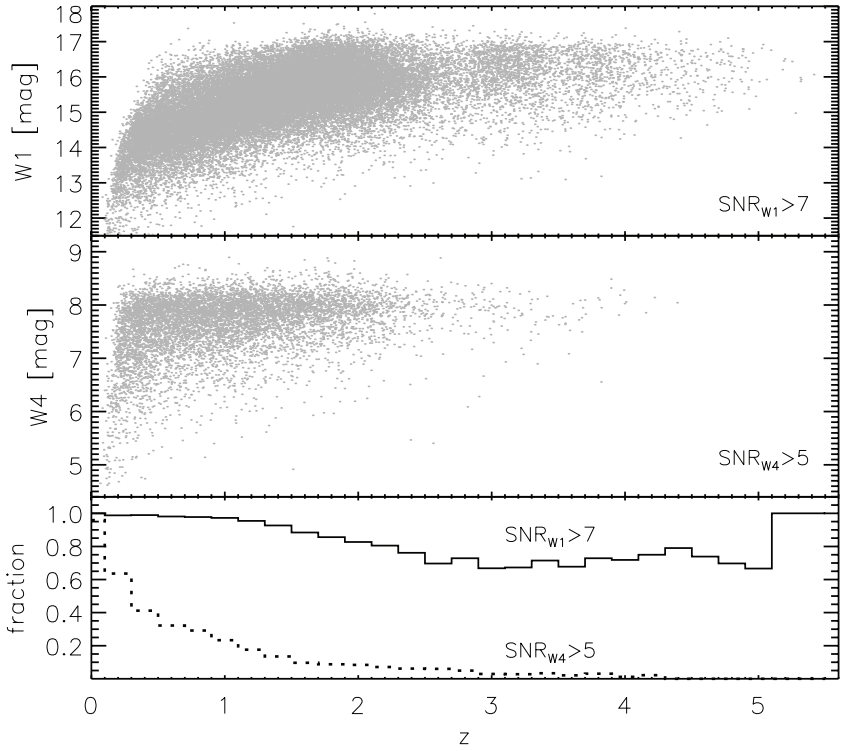

Figure 13. Top two panels show the *WISE* magnitudes ($W1$ and $W4$) as a function of redshift for the SDSS QSO sample (Schneider et al. 2010). As expected, more QSOs are detected at 3.4 μm than at 22 μm. The bottom panel shows the percentages of *WISE*-detected SDSS QSOs as a function of z. The $z > 5.7$ sources are from Fan et al. (2006), Jiang et al. (2009), and CFHT surveys (Willott et al. 2009, 2010).

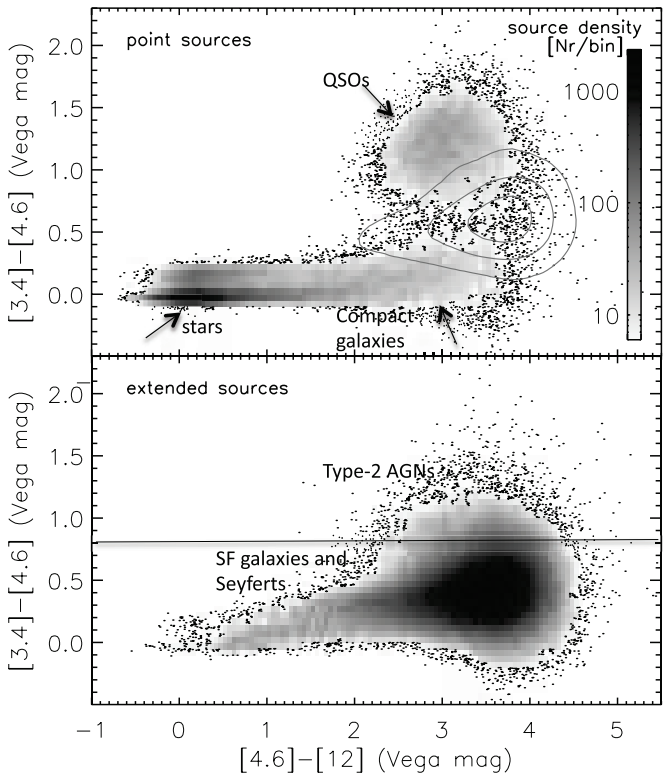

Figure 14. *WISE* colors for SDSS unresolved sources (top panel; SDSS TYPE = 6) and extended galaxies (bottom panel; SDSS TYPE = 3). Comparison of the two panels shows that SDSS point sources have very different $W1 - W2$ and $W2 - W3$ color distributions from that of extended objects. In the top panel, the solid contours represent the distribution of the extended objects shown below. Furthermore, unresolved SDSS sources clearly separate into their two primary constituencies, stars at the origin and quasars with redder colors.

select systems with strong black hole accretions. For fainter type-2 AGN candidates, we use an alternative definition: $W1 - W2 > 0.8$, $W2 < 15.2$, and very red optical-to-mid-infrared color—i.e., optically faint, *WISE* 4.6 μm AGN candidates. As emphasized earlier, when selecting *WISE* AGNs using $W1 - W2$ colors, the $W2 < 15.2$ criterion is very important for limiting contamination from high-redshift galaxies to less than 20% (Assef et al. 2012).

For the former, optically bright type-2 AGN definition, we estimate ~31% of $r < 21$ *WISE*-selected AGNs/QSOs to be spatially resolved. This suggests an almost 2:1 type-1 to type-2 AGN ratio. Since type-2 AGNs here only include bright AGNs with well-resolved host galaxies in optical images, it is not surprising that the type-2 to type-1 ratio is so low—e.g., lower than what is required to explain the hard X-ray background (Gilli et al. 2007; Comastri et al. 2011). With SDSS + *WISE* data, it is also possible to use $r - W2$ color to select type-2 AGNs. Figure 15 examines this technique, showing $r - W2$ colors for both type-1 and optically bright type-2 AGNs with extended SDSS morphologies. The morphological criterion imposes a strong selection function, producing an artificial deficit of luminous type-2 AGN in Figure 15. Higher luminosity sources will tend to be at higher redshifts and high-redshift obscured AGNs drop below the $r = 21$ limit imposed to provide reliable morphologies. Here $L_{12\,\mu m}$ is calculated using spectroscopic or photometric redshifts, including small k-corrections (less than 0.1 mag) based on the appropriate type-1 or type-2 AGN template from Assef et al. (2010). Type-1 and type-2 AGNs clearly have very different $r - W2$ color distributions, especially at the high-luminosity end. This is consistent with what has been found by Hickox et al. (2011) based on X-ray and *Spitzer* data in the Boötes field. This result lends support for using

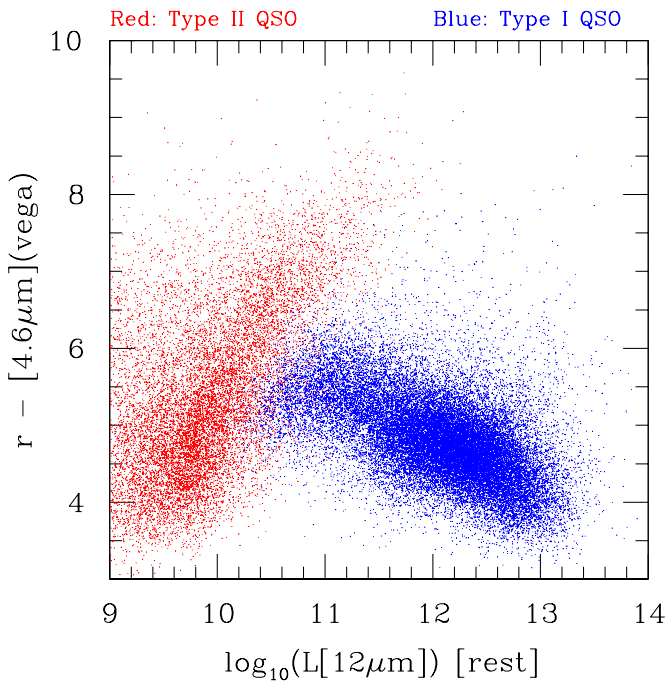

Figure 15. Rest-frame 12 μm luminosity for the optically bright ($r < 21$) AGN sample, including small k-corrections calculated using appropriate SEDs for type-1 (blue) and type-2 (red) AGNs. The differentiation between AGN types is based on optical morphology. The lack of high-luminosity type-2 AGNs is due to the selection effect which uses SDSS extended morphologies as a criterion. More luminous type-2 AGNs will be at higher redshifts where the host galaxy brightness falls below the optical magnitude limit imposed here to ensure reliable morphologies. Likewise, the host galaxies of low-luminosity, broad-lined (type-1) AGNs are likely detected by SDSS, and thus such systems are classified as type-2 AGNs using our morphological criterion.

(A color version of this figure is available in the online journal.)

$r - W2$ to select type-2 AGNs which do not have reliable optical morphology information.

Furthermore, the feasibility of this method is illustrated in Figure 16, showing the calculated optical/mid-IR colors based on assumed sets of SED templates as a function of redshift. These galaxy templates are constrained by actual *Spitzer* observations (Polletta et al. 2007; Vega et al. 2008). We see a strong divergence in optical/mid-IR colors of type-1 and type-2 QSO/AGNs at $z \gtrsim 0.5$. Figure 17 further examines this technique, showing $r - W2$ versus $W1 - W2$ for *WISE* sources with $W2 < 15.2$, matched with SDSS r-band data down to the faintest limits. The secondary branch in the figure shows that sources with red $r - W2$ colors are potential type-2 AGNs. If we use the criteria of $W1 - W2 > 0.8$, $W2 < 15.2$, and $r - W2 > 6$ to define a sample of red AGN as potential type-2 sources, we find that type-2 candidates account for ~29% of all *WISE*-selected AGN candidates to that depth. The surface density of such type-2 AGN candidates is about 16.4 deg^{-2}, whereas $r < 21$ bright with resolved morphology, type-2 AGNs are about 31% of all AGNs, yielding a surface density of 17.3 deg^{-2}. Stern et al. (2012), using the *Hubble Space Telescope* imaging available in the COSMOS field, find that ~50% of *WISE*-selected AGN candidates to a depth of $W2 = 15.2$ are unresolved in I_{814}.

Our intention here is to illustrate the methods of using colors to select large samples of type-2 AGN candidates over wide areas of sky. Our crude estimate of the type-2 AGN fraction (integrated) is on the order of one-third of all AGNs. However, we caution that to truly understand the implications of these numbers, we will need to have the redshift and luminosity information. Such studies utilizing *WISE* plus other ancillary spectroscopic data in smaller regions of sky are included in Assef et al. (2012) and D. Stern et al. (in preparation).

3.4. High-redshift ULIRG Candidates

One of the primary *WISE* mission goals is to identify extremely luminous ($L_{\rm IR} \geqslant 10^{12}$–$10^{13}\,L_{\odot}$) dusty starbursts and AGNs (i.e., ULIRGs and hyperluminous infrared galaxies, or HyLIRGs) at high redshift. We have pursued two basic approaches in finding high-redshift ULIRGs. One is to use *WISE* data alone, and the second is to combine *WISE* with optical data.

Using *WISE* colors alone, high-redshift ULIRGs can be identified by requiring very red, rising mid-infrared SEDs, redder than the spectral index $\alpha \sim -2.56$ corresponding to the *WISE* sensitivity limits (see Section 2.2). Specifically, this means significant detections (S/N > 3–5) in $W3$ or $W4$, but no detections in $W1$ and $W2$, i.e., so-called $W1W2$-dropouts (Eisenhardt et al. 2012). Follow-up optical spectroscopy of more than 100 candidates using the Keck, Gemini, Magellan, and Palomar telescopes has demonstrated that the majority of these candidates are indeed at redshifts of 1–3, implying very high luminosities given the high fluxes at 12 and 22 μm (Eisenhardt et al. 2012; Wu et al. 2012). This type of ULIRG is rare, with a surface density of just 0.02 sources per deg^2. One interesting feature of these ULIRGs is their extremely steep mid-IR spectral slopes. Comparing Figures 10 and 11, we see that the newly discovered *WISE*-selected $z \sim 2$ ULIRGs have much redder $W2 - W3$ colors than the calculated high-z colors using local ULIRG SED templates, including the reddest one such as IRAS 15250+3609. Eisenhardt et al. (2012), Wu et al. (2012), Bridge et al. (2012), and L. Yan et al. (in preparation) present complete discussions on the $W1W2$-drop selection, follow-up spectroscopy, as well as far-infrared photometry from the Caltech Submillimeter Observatory and *Herschel* for some of these extremely luminous ($L_{\rm IR} \sim 10^{13-14}\,L_{\odot}$) ULIRGs at $z \sim 2$.

The second method is to utilize optical/mid-infrared colors. As shown in Figure 16, $r - W1$ color becomes redder at higher redshift. This is true as well for the other three *WISE* bands. Indeed, there is a rich literature using red optical-to-mid-infrared colors with *Spitzer* to select high-redshift galaxies. For example, red 24 μm to r-band colors ($r - [24] > 14$; Vega) have been used in the Extragalactic First Look Survey (XFLS; Yan et al. 2004) and Boötes field to successfully select many highly obscured galaxies at $z \sim 2$ (Yan et al. 2005, 2007; Dey et al. 2008). As shown in Figure 16, highly dust-reddened local ULIRGs, such as IRAS 19254−7245, Mrk 231, UGC5101, and IRAS 08572+3915, have very red colors at any redshifts. Using $r - W4 > 14$ as the selection criterion, *WISE* identifies 0.9 ± 0.07 high-redshift ULIRG candidates per deg^2 for $S/N_{W4} > 5$. This S/N cut roughly corresponds to a 22 μm flux density $\geqslant$2.5 mJy. This is shown in Figure 18. If we instead apply a uniform flux density cut of $f_{\nu}(22\,\mu{\rm m}) \geqslant 5$ mJy, the surface density of ULIRG candidates is 0.41 ± 0.05 deg^{-2}, comparable to that of Dey et al. (2008) using *Spitzer* data over the ~10 deg^{-2} Boötes field with the flux density cut of $f_{\nu}(24\,\mu{\rm m}) \geqslant 5$ mJy. To verify our analysis, we chose a subset of the SDSS−*WISE* overlap region covering 180 deg^2. All of the red, high-redshift candidates with $r - W4 > 14$ were visually examined. We found a small percentage of contaminants (8%). Our derived surface density values have been corrected for this percentage. The *WISE* all-sky data offer an excellent opportunity to assemble

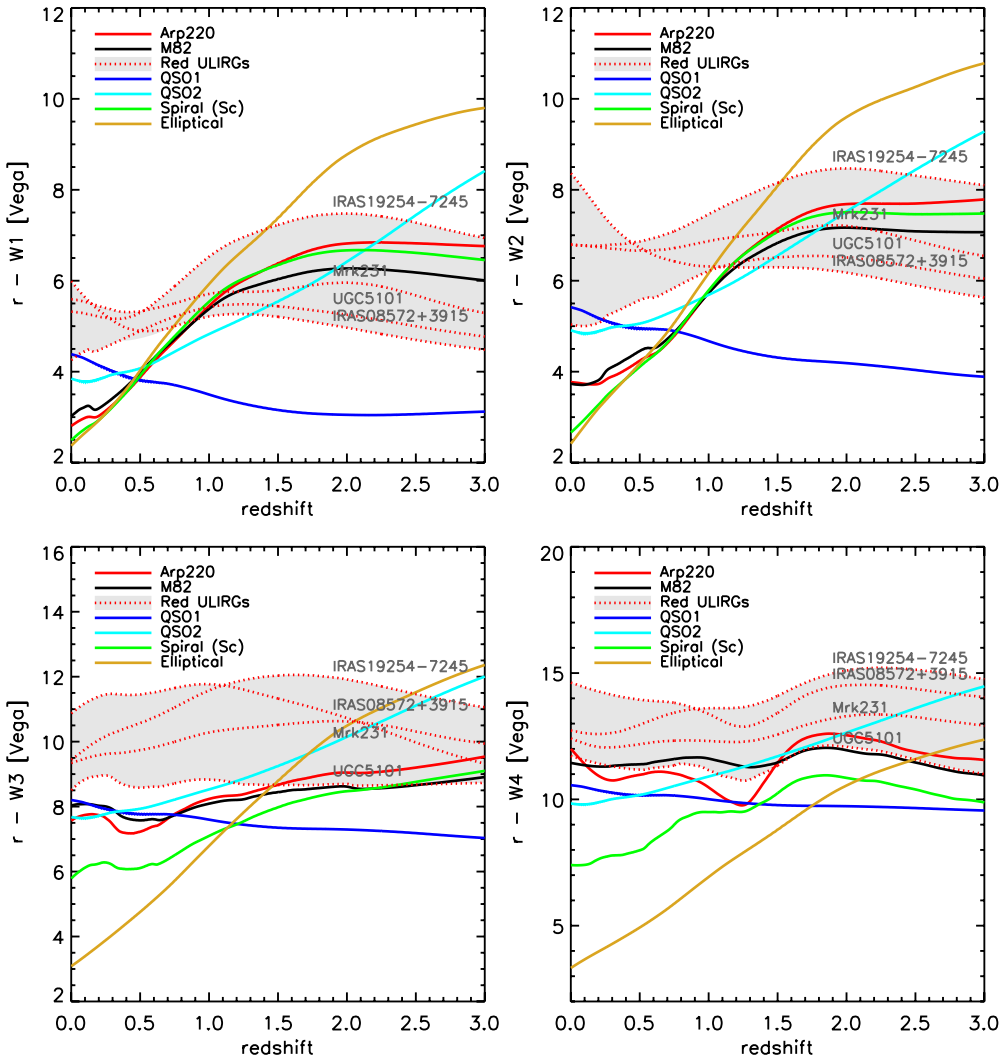

Figure 16. Optical-to-*WISE* color as a function of redshift for a set of galaxy templates. Red ULIRGs refer to local, highly dust-obscured ULIRGs with red mid-infrared SEDs, e.g., Mrk 231 (a type-1 AGN), UGC 5101, IRAS 0872+3915, and IRAS 19254−7245, taken from Polletta et al. (2007) and Vega et al. (2008).

(A color version of this figure is available in the online journal.)

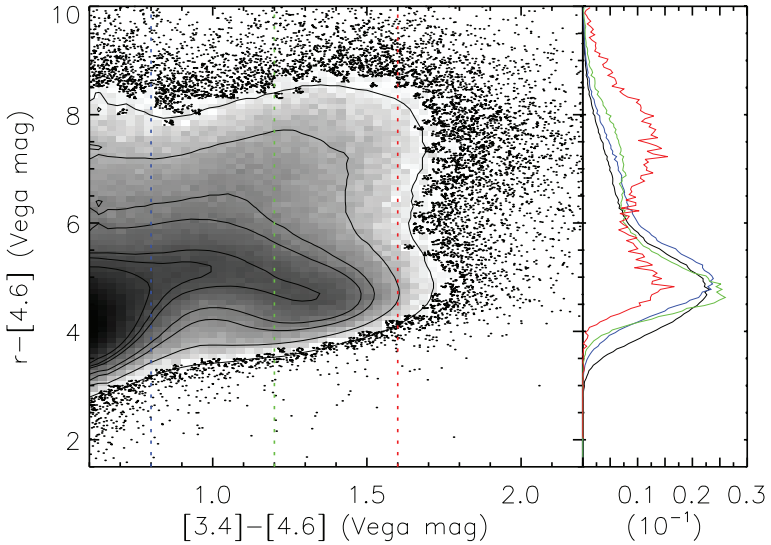

Figure 17. Color–color diagram, plotting $r-W2$ vs. $W1-W2$. Vertical dashed lines show cuts at various $W1-W2$ color; the plot on the right shows the corresponding relative $r-W2$ color distribution for sources redder than those cuts. The right-hand side panel is the histogram of the $r-W2$ color distribution; and the x-axis is the number of objects per $r-W2$ color bin. The black line shows the full source distribution. For red *WISE* sources with $W1-W2>0.8$ (e.g., AGN candidates), two branches are apparent: one with blue colors ($r-W2\sim4.5$) and a secondary branch with $r-W2>6$. We propose that the latter are type-2 AGN candidates.

(A color version of this figure is available in the online journal.)

Table 1
$r - W4 > 14$, High-z Candidates with Optical Spectra

Source	z_{spec}	r^a (mag)	$W3^a$ (mag)	$W4^a$ (mag)	$r - W3$ (mag)	$r - W4$ (mag)	Type
J142228.88+561355.6	2.524	>23.4	9.94 ± 0.03	7.10 ± 0.06	>13.46	>16.30	Type-2 AGN
J145705.91+293231.7	2.908	23.02	9.57 ± 0.03	6.78 ± 0.05	14.45	16.24	Type-1 AGN
J160346.21+362740.2	2.134	>23.4	10.86 ± 0.05	7.38 ± 0.07	>12.54	>16.02	Type-1 AGN
J160456.27+204100.3	1.262	22.48	10.43 ± 0.06	7.69 ± 0.13	12.05	14.79	Type-2 AGN
J161714.90+335556.4	0.619	21.42	9.52 0.03	6.57 ± 0.05	11.90	14.85	Type-2/star forming
J161728.91+233646.8	1.707	22.27	9.02 ± 0.03	6.69 ± 0.07	13.25	15.58	Type-1 AGN
J163619.18+330922.1	0.731	22.64	10.01 ± 0.04	8.00 ± 0.13	12.63	14.64	Type-2 AGN
J170813.71+331538.7	0.773	21.98	9.28 ± 0.03	7.83 ± 0.14	12.70	14.15	Type-2/star-forming

Notes.
[a] All photometry is listed in the Vega system. SDSS r magnitudes have been converted to Vega system by first converting from asinh magnitudes to AB systems, then from AB to Vega.

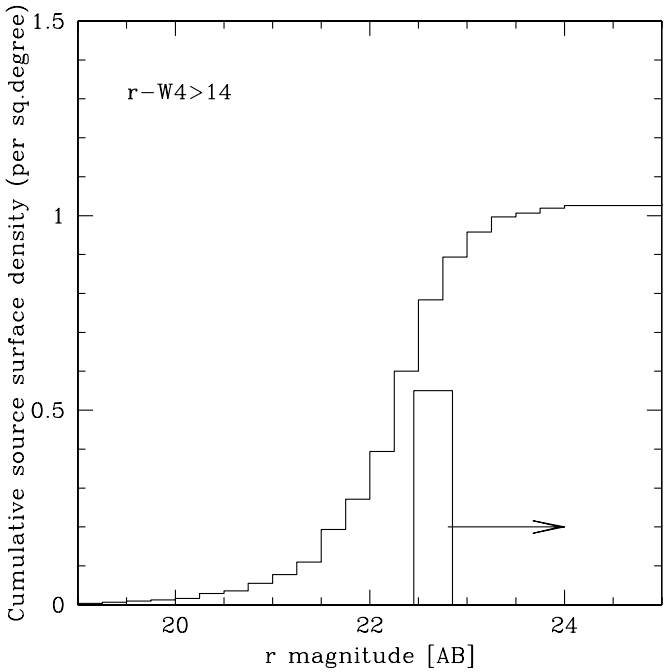

Figure 18. Cumulative surface density of high-redshift ULIRG candidates selected by red optical-to-$W4$ color. The single bar with the right side arrow shows sources without SDSS counterparts.

a large sample of 22 μm selected "dust-obscured galaxies" at $z > 1$–2.

3.5. Keck Spectroscopy of a Sample of High-redshift ULIRG Candidates with Very Red $r - W4$ Color

The *WISE* team has carried out optical spectroscopic follow-up observations of high-redshift ULIRG candidates. These candidates include both $W1W2$-dropouts and extremely red optical/mid-IR sources. Eisenhardt et al. (2012) focused on one particular $W1W2$-dropout, J181417.29+341224.9 at $z = 2.452$, whose optical spectrum shows a typical SF galaxy, whereas its IR SED suggests a highly obscured AGN with a bolometric luminosity of $3.7 \times 10^{13}\ L_{\odot}$. Wu et al. (2012) present optical spectra of a subset of $W1W2$-dropouts with millimeter observations, making a comparison between $W1W2$-dropouts and *Spitzer*-discovered "dust obscured galaxies."

The follow-up observations included a sample of *WISE* sources with $r - W4 \geqslant 14$. Table 1 lists the source information for eight galaxies with good spectra. These spectra were taken using Low Resolution Imager and Spectrograph (LRIS; Oke et al. 1995) on the Keck telescope during the nights of 2011 March 10, April 10, and May 10. The total on-target integration times range from 10 to 15 minutes. Figure 19 shows the wavelength-calibrated spectra in the observed frame for these eight sources. Prominent emission lines include Lyα, C IV λ1549, [Mg II] λ2800, Ne V λ3426, [O II] λ3727, and [O III] λ5007, etc., strong spectral features. W1422+5613 has a C IV λ1549 FWHM of 1480 km s^{-1}, not accounting for the spectral resolution. If we adopt 2000 km s^{-1} for type-1 and type-2 separation based on C IV λ1549, this object is indeed a type-2 AGN. This cutoff value is very conservative compared to the mean C IV λ1549 velocity width of 5600 km s^{-1}, estimated from the SDSS QSO sample (Shen et al. 2008). Similarly, W1457+2932 is a type-1 AGN with a C IV λ1549 FWHM of 3940 km s^{-1}. W1603+3627 has a C IV λ1549 FWHM of 1790 km s^{-1}; however, its C III] λ1909 FWHM is broad, 3170 km s^{-1}, and the [Mg II] λ2800 is broad as well. Since C IV λ1549 line is a complex line and could have some absorption. We classify this object as type-1 based on C III] λ 1909 and [Mg II] λ2800 instead. W1604+2041 is a type-2 AGN with a Ne V λ3426 FWHM of 1350 km s^{-1}. W1617+3355 has a ratio of [O III] λ5007 to Hβ of 3.7, which is in a range that could be either AGN or SF based on the Baldwin, Phillips & Terlevich (BPT) diagram. Its [O III] λ5007 FWHM is 610 km s^{-1}, making it consistent with either a type-2 AGN or an SF galaxy. W1617+2336 is a type-1 AGN with a C IV λ1549 FWHM of 4800 km s^{-1}. W1636+3309 has a ratio of [O III] λ5007 to Hβ > 20, which implies an AGN; however, the available spectral line widths for a small number of features are narrow, suggesting it to be a type-2. The classification for this source is not clear. W1708+3315 has [O III]/Hβ = 3.0, again making it ambiguous, either a type-2 AGN or an SF galaxy. Table 1 lists these classifications. Although the number of spectra is small and there are some ambiguous systems, the source types among the randomly selected eight targets are dominated by type-2 AGNs. This supports the interpretation that the high mid-IR fluxes at 22 μm are due to dust emission heated by obscured central AGNs.

We plot the colors and brightness of these eight sources as a function of their spectroscopic redshifts in Figure 20. It suggests that optically fainter or $r - W4$ redder candidates could be at higher redshifts. The brightness in the 22 μm band does not appear to correlate with redshift, with many high-redshift ULIRGs being quite bright in W4.

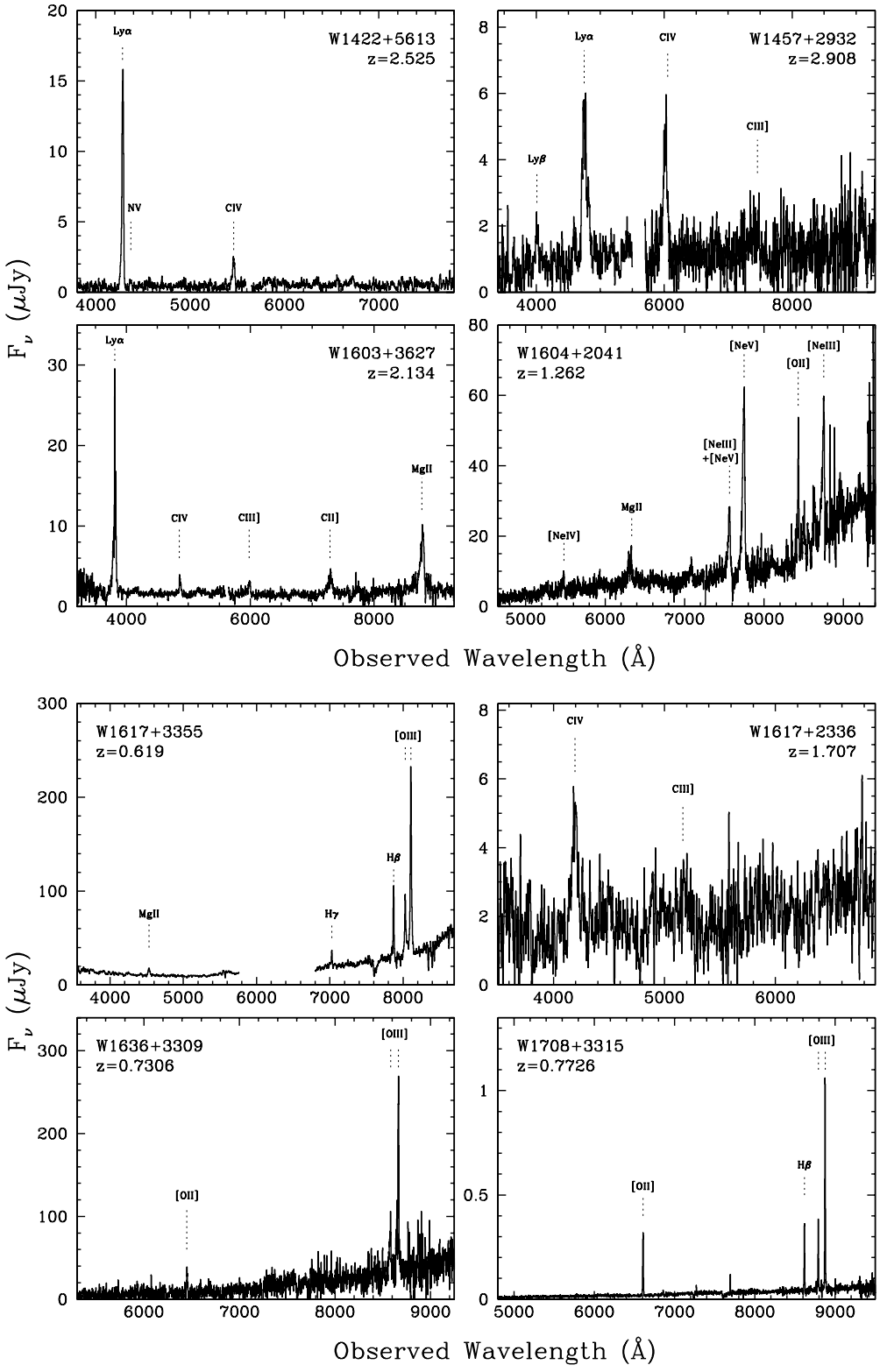

Figure 19. Optical spectra of the high-redshift ULIRG candidates selected by $r - W4 > 14$.

4. DISCUSSION AND SUMMARY

With the public data releases, *WISE* has delivered to the community the most sensitive all-sky mid-infrared map of our generation. In this paper, we present a phenomenological study that characterizes the observational properties of mid-infrared extragalactic sources and identifies color selection criteria for isolating large samples of QSOs, dust-obscured type-2 AGNs and luminous high-redshift ULIRG candidates.

With 5σ sensitivities $\leqslant$0.05, 0.1, 0.75, and 6 mJy at 3.4, 4.6, 12, and 22 μm, the $W1$, $W1/2$, $W1/2/3$, and $W1/2/3/4$ samples have source surface densities of 8230, 4700, 1235, and 150 deg^{-2}, respectively. At the limit of the data, only very red mid-infrared sources with spectral slopes steeper than

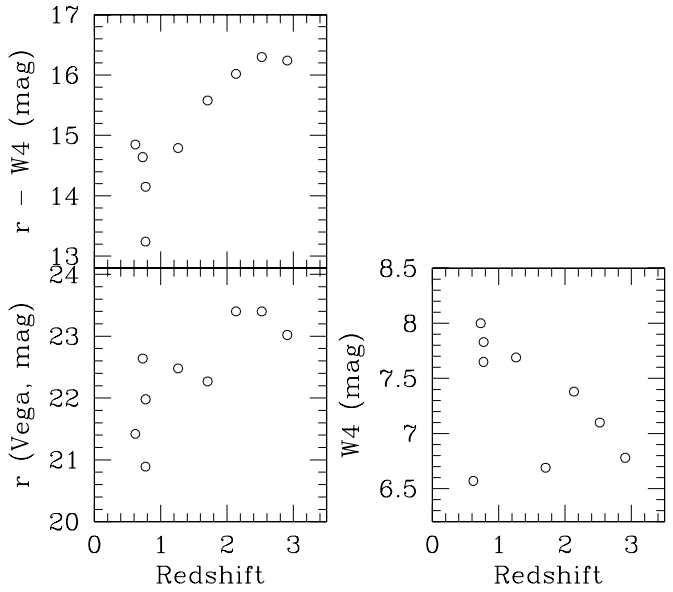

Figure 20. Colors and brightness as a function of redshift for the 8 $r-W4>14$ ULIRG candidates with spectroscopic redshifts. The three panels are intended to investigate trends for selecting high-redshift ULIRG candidates. It is clear that fainter optical magnitudes or redder $r-W4$ colors seem to select ULIRGs at higher redshifts.

~ -2.56 are simultaneously detected in both $W1$ and $W4$. The $W1$ source density is one-third that of the SDSS photometric catalog, suggesting that *WISE* 3.4 μm does not detect many low-mass, low-luminosity, blue galaxies (Donoso et al. 2012). We find that 28% of the $W1$ sample have r-band magnitudes fainter than 22.6, including many sources lacking optical counterparts. We present observational evidence that suggests that optically faint 3.4 μm sources are likely early-type galaxies beyond the redshift limit of the SDSS imaging data.

WISE 3.4 μm data are sensitive to bright quasars. Of the entire SDSS optical QSO sample (Schneider et al. 2010), 89.8% have $W1$ detections at S/N >7. *WISE* even detects 3.4 μm emission from the highest known redshift QSO, ULAS J1120+0461 at $z=7.085$ (Mortlock et al. 2011). In contrast, only 18.9% of all SDSS QSO samples have $W4$ detections at S/N >5. Some of these optically selected bright QSOs detected at 22 μm are not just bright in all bands, but indeed have strong mid-IR dust emission.

The unique advantage of *WISE* all-sky data for extragalactic sources is the diagnostic power of its mid-infrared colors. This power comes from the fact that pure stellar systems, SF galaxies, and QSOs/AGNs have distinctly different near-infrared SEDs (see Figure 9), yielding very different observed mid-infrared colors for different types of objects. We show that *WISE* colors alone can separate source populations, including Galactic stars, SF galaxies, and QSO/AGN. We present three useful applications of *WISE* all-sky data. (1) We select QSOs/strong AGNs at $z<3$ using $W1-W2$ color and $W2<15.2$. The magnitude cut is to limit the contamination from early galaxies at high redshift. This population of QSOs is interesting to inventory since a large fraction of QSOs at $z\sim 2$–3 are missed by the SDSS optical color selection. Beyond $z\sim 3$, the *WISE* QSO color selection starts to fail as the 3.4 μm and 4.6 μm bands sample wavelengths blueward of 1 Å, and the observed *WISE* colors start to have overlap with low-redshift SF galaxies. (2) We demonstrate the possibility for selecting type-2 AGN/QSO candidates using $W1-W2>0.8$, $W2<15.2$, and $r-W2>6$ (or SDSS optically resolved morphologies for $r<21$ sources). The *WISE* data allow a more complete census of dust-obscured, actively accreting, supermassive black hole systems than allowed by the current generation of deep X-ray surveys. (3) High-redshift ($z>2$) dust-obscured, extremely luminous ULIRGs/HyLIRGs are another population of extragalactic objects which the *WISE* data can be used to identify. With follow-up optical spectroscopy, Eisenhardt et al. (2012) demonstrate the efficient selection of $z\sim 2$–3 ULIRGs with extremely red mid-infrared slopes (the $W1W2$-dropout method). In addition, we show that extremely red optical-to-mid-IR colors, e.g., using $r-W4>14$, can also be used to select high-redshift dust-obscured starbursts and AGNs. The candidate surface density for this later selection is 0.9 ± 0.07 at S/N$_{W4}>5$. This is consistent with the number inferred from the previous studies using *Spitzer* data over much smaller areas.

Optical spectroscopic follow-up of a small number of $r-W4>14$ ULIRG candidates confirms that the color selection indeed works, identifying IR luminous galaxies over a wide range of redshift, $z\sim 0.7$–3. Despite small number statistics, we find indications that optically fainter and $r-W4$ redder sources tend to be at higher redshifts. The Keck optical spectra for the eight sources detect many typical strong emission nebular lines seen among AGNs, such as Lyα, C IV λ1549, Ne V λ3426, and [O III] λ5007 lines. In addition, of the eight sources with the optical spectra, five have spectral types of type-2 AGNs, one type-1 AGN with a fairly broad C IV λ1549 emission line, and two possible SF galaxies.

This publication makes use of data products from the *Wide-field Infrared Survey Explorer*, which is a joint project of the University of California, Los Angeles, and the Jet Propulsion Laboratory/California Institute of Technology, funded by the National Aeronautics and Space Administration. This paper also utilized the publicly available SDSS data sets. Funding for the SDSS and SDSS-II has been provided by the Alfred P. Sloan Foundation, the Participating Institutions, the National Science Foundation, the US Department of Energy, the National Aeronautics and Space Administration, the Japanese Monbukagakusho, the Max Planck Society, and the Higher Education Funding Council for England. The SDSS Web site is http://www.sdss.org/. The SDSS is managed by the Astrophysical Research Consortium for the Participating Institutions. The Participating Institutions are the American Museum of Natural History, Astrophysical Institute Potsdam, University of Basel, University of Cambridge, Case Western Reserve University, University of Chicago, Drexel University, Fermilab, the Institute for Advanced Study, the Japan Participation Group, Johns Hopkins University, the Joint Institute for Nuclear Astrophysics, the Kavli Institute for Particle Astrophysics and Cosmology, the Korean Scientist Group, the Chinese Academy of Sciences (LAMOST), Los Alamos National Laboratory, the Max-Planck-Institute for Astronomy (MPIA), the Max-Planck-Institute for Astrophysics (MPA), New Mexico State University, Ohio State University, University of Pittsburgh, University of Portsmouth, Princeton University, the United States Naval Observatory, and the University of Washington. Some of the data presented herein were obtained at the W. M. Keck Observatory, which is operated as a scientific partnership among the California Institute of Technology, the University of California, and the National Aeronautics and Space Administration. The Observatory was made possible by the generous financial support of the W. M. Keck Foundation. The authors recognize and acknowledge the

very significant cultural role and reverence that the summit of Mauna Kea has always had within the indigenous Hawaiian community. We are most fortunate to have the opportunity to conduct observations from this mountain.

REFERENCES

Abazajian, K. N., Adelman-McCarthy, J. K., Agüeros, M. A., et al. 2009, ApJS, 182, 543
Ashby, M., Stern, D., Brodwin, M., et al. 2009, ApJ, 701, 428
Assef, R. J., Kochanek, C. S., Brodwin, M., et al. 2010, ApJ, 713, 970
Assef, R. J., Stern, D., Kechanek, C. S., et al. 2012, ApJ, submitted (arXiv:1209.6055)
Becker, R. H., White, R. L., & Helfand, D. J. 1995, ApJ, 450, 559
Blain, A. W., Assef, R., Stern, D., et al. 2013, ApJ, submitted
Bridge, C., Blain, A. W., Borys, C. J. K., et al. 2012, ApJ, submitted (arXiv:1205.4030)
Brinchmann, J., Charlot, S., White, S. D. M., et al. 2004, MNRAS, 351, 1151
Brodwin, M., Brown, M. J. I., Ashby, M. L. N., et al. 2006, ApJ, 651, 791
Comastri, A., Ranalli, P., Iwasawa, K., et al. 2011, A&A, 526, L9
Cutri, R., Wright, E. L., Conrow, T., et al. 2011, Explanatory Supplement to the *WISE* Preliminary Data Release Products, http://wise2.ipac.caltech.edu/docs/release/prelim/expsup/
Dey, A., Soifer, B. T., Desai, V., et al. 2008, ApJ, 677, 943
Donoso, E., Yan, L., Tsai, C.-W., et al. 2012, ApJ, 748, 80
Eckart, M., McGreer, I., Stern, D., et al. 2010, ApJ, 708, 584
Edelson, R., & Malkan, M. 2012, ApJ, 751, 52
Eisenhardt, P. R. M., Brodwin, M., Gonzalez, A. H., et al. 2008, ApJ, 684, 905
Eisenhardt, P. R. M., Wu, J., Tsai, C.-W., et al. 2012, ApJ, 755, 173
Eisenstein, D. J., Annis, J., Gunn, J. E., et al. 2001, AJ, 122, 2267
Fan, X., Strauss, M. A., Becker, R. H., et al. 2006, AJ, 132, 117
Fukugita, M., Shimasaku, K., & Ichikawa, T. 1995, PASP, 107, 945
Galametz, A., Stern, D., De Breuck, C., et al. 2012, ApJ, 749, 169
Gettings, D., Gonzalez, A. H., Stanford, S. A., et al. 2012, ApJL, 759, 23
Gilli, R., Comastri, A., & Hasinger, G. 2007, A&A, 463, 79
Griffith, R., Tsai, C.-W., Stern, D., et al. 2011, ApJL, 736, 22
Hickox, R., Myers, A. D., Brodwin, M., et al. 2011, ApJ, 731, 117
Jarrett, T., Cohen, M., Masci, F., et al. 2011, ApJ, 735, 112
Jarrett, T., Masci, F., Tsai, C. W., et al. 2013, AJ, 145, 6
Jiang, L., Fan, X., Bian, F., et al. 2009, AJ, 138, 305
Jiang, L., Fan, X., Brandt, W. N., et al. 2010, Natur, 464, 380
Kauffmann, G., Heckman, T. M., Tremonti, C., et al. 2003, MNRAS, 346, 1055
Kewley, L. J., Dopita, M. A., Sutherland, R. S., Heisler, C. A., & Trevena, J. 2001, ApJ, 556, 121
Kirkpatrick, J. D., Cushing, M. C., Gelino, C. R., et al. 2011, ApJS, 197, 19
Lacy, M., Storrie-Lombardi, L. J., Sajina, A., et al. 2004, ApJS, 154, 166
Lake, S., Wright, E. L., Petty, S., Assef, R. J., Jarrett, T. H., Stanford, S. A., Stern, D., & Tsai, C.-W. 2012, AJ, 143, 7
Lin, Y.-T., Mohr, J. J., & Stanford, S. A. 2004, ApJ, 610, 745
Mancone, C., Gonzalez, A., Brodwin, M., et al. 2010, ApJ, 720, 284
Massaro, F., D'Abrusco, R., Tosti, G., et al. 2012, ApJ, 750, 138
Mateos, S., Alonso-Herrero, A., Carrera, F. J., et al. 2012, MNRAS, 426, 3271
Mortlock, D. J., Warren, S. J., Venemans, B. P., et al. 2011, Natur, 474, 616
Neugebauer, G., Habing, H. J., van Duinen, R., et al. 1984, ApJL, 278, 1
Oke, J. B., Cohen, J. G., Carr, M., et al. 1995, PASP, 107, 375
Oyaizu, H., Lima, M., Cunha, C. E., et al. 2008, ApJ, 674, 768
Petrosian, V. 1976, ApJL, 209, 1
Polletta, M., Tajer, M., Maraschi, L., et al. 2007, ApJ, 663, 81
Richards, G. T., Fan, X., Newberg, H. J., et al. 2002, AJ, 123, 2945
Schneider, D. P., Richards, G. T., Hall, P. B., et al. 2010, AJ, 139, 2360
Scoville, N., Abraham, R. G., Aussel, H., et al. 2007, ApJS, 172, 38
Shen, Y., Greene, J. E., Strauss, M. A., Richards, G. T., & Schneider, D. P. 2008, ApJ, 680, 169
Skrutskie, M. F., Cutri, R. M., Stiening, R., et al. 2006, AJ, 131, 1163
Stern, D., Assef, R. J., Benford, D. J., et al. 2012, ApJ, 753, 30
Stern, D., Eisenhardt, P., Gorjian, V., et al. 2005, ApJ, 631, 163
Stoughton, D., Lupton, R. H., Bernardi, M., et al. 2002, AJ, 123, 485
Tsai, C. W., Jarrett, T. H., Stern, D., et al. 2013, ApJ, submitted
Vega, O., Clemens, M. S., Bressan, A., et al. 2008, A&A, 484, 631
Willott, C. J., Delorme, P., Reylé, C., et al. 2009, AJ, 137, 3541
Willott, C. J., Delorme, P., Reylé, C., et al. 2010, AJ, 139, 906
Wright, E. L., Eisenhardt, P. R. M., Mainzer, A. K., et al. 2010, AJ, 140, 1868
Wu, J., Tsai, C.-W., Sayers, J., et al. 2012, ApJ, 756, 96
Wu, X.-B., Hao, G., Jia, Z., Zhang, Y., & Peng, N. 2012, AJ, 144, 49
Yan, L., Chary, R., Armus, L., et al. 2005, ApJ, 628, 604
Yan, L., Choi, P. I., Fadda, D., et al. 2004, ApJS, 154, 75
Yan, L., Sajina, A., Fadda, D., et al. 2007, ApJ, 658, 778